DOI: https://doi.org/10.2138/am-2019-6602

Revision 2

Application of Mineral Equilibria to Estimate Fugacities of H_2O, H_2 and O_2 in Mantle Xenoliths from the SW USA

Lindsey E. Hunt

Electron Microprobe Laboratory
Office of the Vice President for Research
University of Oklahoma,
Norman, OK 73069, U.S.A

William M Lamb

Dept. of Geology & Geophysics
Texas A&M University,
College Station, TX 77843, U.S.A

Running Title: Constraining mantle fluids using mineral equilibria

Email: w-lamb@geos.tamu.edu

Phone: 979-492-5800

This is a preprint, the final version is subject to change, of the American Mineralogist (MSA)
Cite as Authors (Year) Title. American Mineralogist, in press.
DOI: https://doi.org/10.2138/am-2019-6602

Revision 2

ABSTRACT

Small amounts of H_2O, on the order of 10's to 100's ppm, can significantly influence the physical properties of mantle rocks. Determining the H_2O contents of nominally anhydrous minerals (NAMs) is one, relatively common, technique that has been applied to estimate mantle H_2O contents. However, for many mantle NAMs, the relation between H_2O activity and H_2O content is not well known. Furthermore, certain mantle minerals may be prone to H_2O loss during emplacement on Earth's surface. The goal of this study is to apply mineral equilibria to estimate values of aH_2O in rocks that originated below the Moho.

The chemical compositions of olivine + orthopyroxene + clinopyroxene + amphibole + spinel ± garnet were used to estimate values of temperature (T), pressure (P), aH_2O, hydrogen fugacity (fH_2), and oxygen fugacity (fO_2) in 11 amphibole-bearing mantle xenoliths from the southwestern U.S.A. Application of amphibole dehydration equilibria yields values of aH_2O ranging from 0.05 to 0.26 for these 11 samples and the compositions of coexisting spinel + olivine + orthopyroxene yield $\Delta\log fO_2$ (FMQ) of -1 to +0.6. For nine of the samples, values of fH_2 were estimated using amphibole dehydrogenation equilibria, and these values of fH_2 ranged from 6 to 91 bars. Values of fH_2 and fO_2 were combined, using the relation $2H_2O = 2H_2 + O_2$, to estimate a second value of aH_2O that ranged from 0.01 to 0.57 for these nine samples. Values of aH_2O, estimated using these two methods on the same sample, generally agree to within 0.05. This agreement indicates the amphiboles in these samples have experienced little or no retrograde H-loss and that amphibole equilibria yields robust estimates of aH_2O that, in these xenoliths, are generally less than 0.3, and are often 0.1 or less.

KEYWORDS: amphibole; fluids; mantle; xenoliths; mineral equilibria;

This is a preprint, the final version is subject to change, of the American Mineralogist (MSA)
Cite as Authors (Year) Title. American Mineralogist, in press.
DOI: https://doi.org/10.2138/am-2019-6602

Revision 2

INTRODUCTION

Trace amounts of H_2O can significantly affect the physical properties of the upper mantle, including electrical conductivity and rheology (Karato et al., 1986; Bell & Rossman, 1992; Kohlstedt et al., 1995; Mei & Kohlstedt, 2000b, a; Bolfan-Casanova, 2005; Wang et al., 2006; Yoshino et al., 2009; Zhao & Yoshino, 2016). Also, the compositions of melts generated in the mantle are a function of pressure, temperature, and H_2O fugacity (Wyllie, 1979; Gaetani & Grove, 1998; Green & Falloon, 1998; Green, 2015). Thus, the determination of values of the activity of H_2O (aH_2O) for samples from the upper mantle should yield additional insight into various mantle processes.

Molecular H_2O is the dominant form of water or water-vapor in the Earth's hydrosphere, however, in the deeper portions of the Earth much of the hydrogen may be incorporated as various species in minerals and melts. In these cases (minerals and melts) the dominant H-bearing species may be more accurately described as H (hydrogen), and not molecular H_2O. Although, this H may, in many cases, be bonded to an oxygen and, in these cases, the H-bearing species may be referred to as OH. If a volatile-rich fluid is present, a significant fraction may be molecular H_2O, however, under reducing conditions, CH_4 may be the dominant H-bearing species (e.g., French, 1966; Kang et al., 2017). In this paper we prefer to use H_2O as a general term meant to reflect both H_2O that occurs in a volatile-rich fluid and H or OH that occurs in melts or is incorporated in the structures of minerals. However, we sometimes choose to emphasize that the H_2O in question is bound in a mineral and, therefore, may refer to the OH content of amphibole (or other "hydrous" minerals) or the H-contents of nominally anhydrous phases.

This is a preprint, the final version is subject to change, of the American Mineralogist (MSA)
Cite as Authors (Year) Title. American Mineralogist, in press.
DOI: https://doi.org/10.2138/am-2019-6602

The H_2O content of mantle is typically inferred from the H_2O content of nominally anhydrous minerals (NAMs) such as olivines and pyroxenes (Ingrin & Skogby, 2000; Beran & Libowitzky, 2006; Skogby, 2006; Peslier, 2010; Warren & Hauri, 2014). However, NAMs may also undergo substantial resetting of hydrogen contents during xenolith transport and emplacement on the Earth's surface (Ingrin et al., 1995; Kohlstedt & Mackwell, 1998; Ingrin & Skogby, 2000; Demouchy et al., 2006; Peslier & Luhr, 2006). This potential H_2O-loss constitutes a significant uncertainty in determining the amount of H_2O actually stored in NAMs throughout the mantle. Obviously, determining values of mantle aH_2O from the H_2O content of NAMs requires that NAMs have retained their mantle H_2O content during transport and emplacement at the Earth's surface and, furthermore an accurate description of the relation between aH_2O and NAM H_2O content must be available.

Determining a value of aH_2O from the H_2O content of olivine is not straightforward in part because the solubility of OH in olivine depends on a number of variables, including the fugacity of H_2O (fH_2O), P, and T, oxygen fugacity, and olivine composition. For example, early work quantified the relation between olivine OH concentration, fH_2O, P, T (Kohlstedt et al., 1996; Mosenfelder et al., 2006), and the Fe-content of olivine (Zhao et al., 2004). However, it was recognized that other variables, such as oxygen fugacity (Grant et al., 2007) and the abundances of certain trivalent cations (Berry et al., 2007), might also play a significant role in the solubility of hydrous species in olivine. More recent work has combined many of these variables and may, therefore, provide reasonable estimates of the H content of olivine if P, T, fH_2O, fO_2 and the composition of the olivine have been quantified (Gaetani et al., 2014). These same factors (i.e. P, T, fH_2O, and crystal chemistry) also affect the solubility of H_2O in ortho- and clinopyroxenes (Smyth et al., 1991; Mierdel & Keppler, 2004; Stalder, 2004; Smyth et al., 2007; Bali et al., 2008;

Stalder et al., 2008; Warren & Hauri, 2014). However, the relationship between fugacity of H_2O and pyroxene H_2O content is not well known, thus making the determination of values of aH_2O from pyroxene H_2O content difficult as compared to olivine. This is particularly unfortunate given that pyroxenes may be more resistant to resetting during emplacement on Earth's surface (Peslier et al., 2002; Bolfan-Casanova, 2005; Ingrin, 2006; Peslier, 2010; Warren & Hauri, 2014).

Mineral equilibria provide another approach to ascertain the nature of mantle fluids, and various equilibria have been successfully applied to estimate values of P, T, aH_2O, oxygen fugacity (fO_2), and hydrogen fugacity (fH_2) in samples from the Earth's mantle (Nickel & Green, 1985; Wood, 1990; Taylor, 1998; Popp et al., 2006; Lamb & Popp, 2009; Nimis & Grütter, 2010; Miller et al., 2016). Values of oxygen fugacity (fO_2) have been estimated using mineral equilibria based on coexisting olivine, spinel and orthopyroxene (Wood, 1990; Ballhaus et al., 1991; Woodland et al., 1992; Miller et al., 2016). Amphibole dehydrogenation equilibria have been used to estimate values of hydrogen fugacity (fH_2), which can be combined with values of fO_2 from the same sample to estimate aH_2O (Popp & Phillips, 1995; Popp et al., 2006). Amphibole dehydration equilibria have also been used to estimate values of aH_2O (Lamb & Popp, 2009; Bonadiman et al., 2014; Gentili et al., 2015; Kang et al., 2017). The goal of this study is to use mineral equilibria to estimate the fugacities of various fluid species in mantle xenoliths from the SW U.S.A and, in particular, to determine robust values of aH_2O.

This study relies on amphibole-bearing xenoliths that originated below the Moho. Although amphibole may be ubiquitous in the uppermost mantle (Niida & Green, 1999), mantle amphibole often forms as a result of mantle metasomatism (O'Reilly & Griffin, 2013). They can also form as cumulates directly from magmas crystallizing deep within the Earth (Best, 1970; Best, 1975; Irving, 1980; Perkins & Anthony, 2011). Amphibole originating from different enviroments may

also exhibit many different textures that may be useful to interpretating the conditions of formation. For example, they may grow as poikilitic grains that comprise the matrix of a particular sample, or they may appear as veins, or as rims around other mineral grains, such as pyroxene and/or spinel. It has been suggested that, in some cases, mantle amphiboles form from relatively oxidizing fluids (Dyar et al., 1993) and that amphibole-bearing mantle samples tend to record fO_2 values that are, in general, relatively oxidizing (Bryndzia & Wood, 1990). Quantifying values of aH_2O and fO_2 in amphibole-bearing mantle xenoliths that originated from different environments may, therefore, provide insight into the nature of mantle fluids and also test the possibility that the presence of amphibole indicates relatively oxidizing conditions.

ANALYTICAL METHODS

Electron Microprobe

The minerals in these xenoliths were characterized using a Cameca SX-50 electron microprobe (EMP) located at Texas A&M University. Typical operating conditions include an accelerating voltage of 15 kV, and, in the case of anhydrous phases, (e.g., olivine, spinel and pyroxenes) a 20 nA beam current and a 1μm beam diameter. Amphibole is analyzed using a lower beam current of 10 nA and a larger beam diameter of 10 μm in an effort to minimize electron-beam induced diffusion of light elements. Counting times for all phases ranged from 30-60 s for major elements and up to 120 s for minor elements. Typically, a series of points are analyzed along a traverse from core to rim to quantify the chemical variability within mineral grains. Olivine and spinel analyses have been normalized to three cations, while pyroxenes were normalized to four cations and garnets were normalized to eight cations. Natural and synthetic mineral standards are used for calibration. Mineral analyses can be found in Tables 1-5 and Electronic Appendices 2-7.

Complete characterization of mineral chemistries requires the determination of values of Fe^{3+}/Fe_{Total} (where $Fe_{Total} = Fe^{3+} + Fe^{2+}$). However, conventional EMP analyses cannot differentiate between the two common valence states of Fe. In this study, it is assumed that all Fe in olivine is Fe^{2+}, because olivine analyses indicate that this mineral never contains more than trace levels of Fe^{3+} (Brown, 1980). The other minerals that were chemically characterized for this study may contain significant amount of Fe^{3+}. Values of Fe^{3+}/Fe_{Total} for these minerals can be estimated using the EMP either by charge balance (e.g., Droop, 1987; Quinn et al., 2016), or by quantifying some characteristic of the Fe Lα and/or Fe Lβ peaks as a function of the value of Fe^{3+}/Fe_{Total} in certain minerals (e.g., Albee & Chodos, 1970; Höfer et al., 1994; Fialin et al., 2001; Fialin et al., 2004; Lamb et al., 2012).

Determining values of Fe^{3+}/Fe_{Total} in minerals via charge balance requires analytical precision (reproducibility) and accuracy that may, in some cases, be difficult to achieve using the EMP (Canil & O'Neill, 1996). For example, EMP analyses are sufficiently precise to determine values of Fe^{3+}/Fe_{Total} in spinels using charge balance, at least for spinels with compositions similar to those typically found in the mantle (Wood & Virgo, 1989b; Canil & O'Neill, 1996). Although the precision is sufficient, accurate values of Fe^{3+}/Fe_{Total} for these spinels may require correction based on analyses of secondary standards in which Fe^{3+}/Fe_{Total} contents determined independently (Wood & Virgo, 1989b; Davis et al., 2017). We applied this approach to quantify the ferric-ferrous ratio of Fe in the spinels analyzed for this study using secondary standards obtained from B. Wood (Wood & Virgo, 1989b; Ionov & Wood, 1992), which have values of Fe^{3+}/Fe_{Total} determined using Mößbauer spectroscopy (see Wood & Virgo, 1989b).

In contrast to mantle spinels, it has been argued that determining values of Fe^{3+}/Fe_{Total} in pyroxenes via charge balance requires analytical precision (reproducibility) that is not typically

realized using the EMP (Canil & O'Neill, 1996). However, replicate analyses on individual orthopyroxenes, and multiple orthopyroxenes, from the samples examined in this study indicates that the analytical precision is sufficient to reveal significant differences in values of Fe^{3+}/Fe_{Total} between orthopyroxenes contained in different samples. These orthopyroxene analyses are summarized in Table 4 of the supplemental data and all samples, with one exception (sample Ba-1-72 with Fe^{3+}/Fe_{Total} of 0.49), have average values of Fe^{3+}/Fe_{Total} ranging from 0.01 to 0.27, with 1σ standard deviation ≤ 0.04 for all samples. Values of Fe^{3+}/Fe_{Total} are also depicted on a histogram (Figure 1) which plots Fe^{3+}/Fe_{Total} estimated for each orthopyroxene analysis based on charge balance (where $Fe^{3+} = Al^{IV} - Al^{VI} - 2Ti - Cr + Na$) and illustrates that significant differences exist between samples. Thus, for the orthopyroxenes examined in this study, charge balance using the EMP can differentiate between samples at a level of 0.1 or better.

The average values of Fe^{3+}/Fe_{Total} estimated for orthopyroxenes in six samples are approximately 0.1 or less. These values are similar to those determined for mantle orthopyroxenes using Mößbauer spectroscopy (Dyar et al., 1989; Canil & O'Neill, 1996). However, some values reported here are greater than 0.1, with four ratios of Fe^{3+}/Fe_{Total} that are > 0.2. Thus, ratios of Fe^{3+}/Fe_{Total} may be overestimated, and without pyroxenes with independently determined values of Fe^{3+}/Fe_{Total}, which could be used as secondary standards, systematic uncertainties are possible. The same argument may be applied to the clinopyroxene analyses as the estimates of Fe^{3+}/Fe_{Total} (Table 3) may suffer from systematic uncertainties. Thus, we have estimated the value of Fe^{3+}/Fe_{Total} for orthopyroxene and clinopyroxenes, using two methods: (1) charge balance, which, in this case, may yield maximum values, and, (2) assuming that all Fe is Fe^{2+} (a minimum value). This approach permits an examination of the sensitivity of various estimates (e.g., T and fO_2, described below), to changes in the value of Fe^{3+}/Fe_{Total} in pyroxenes.

Complete characterization of amphibole chemistry requires determination of: (1) the H_2O content, (2) the value of Fe^{3+}/Fe_{Total}, and (3) the fraction of the A-site that is vacant. Because conventional microprobe analyses do not provide this information, normalizing amphibole formulae may require certain assumptions regarding numbers of cations and site occupancies (Spear, 1995, p 103-105). In this study, the Fe^{3+}/Fe_{Total} of the amphiboles from nine of the samples have been measured using the Fe Lα peak shift method, as described in Lamb et al. (2012). This calibration is limited to amphibole compositions with ≥ 5 wt. % FeO (Lamb et al., 2012). Consequently, the Fe^{3+}/Fe_{Total} of the amphibole from samples Ba2-1-1 and TF6 have not been determined using this method (see Table 2), and, in these two cases, the chemical formulae of the amphiboles were determined by fixing $Fe^{3+}/Fe_{Total} = 0$. This choice, $Fe^{3+}/Fe_{Total} = 0$, generates a maximum value of aH_2O when estimated using amphibole dehydration equilibria (as described in subsequent sections of this paper). The OH contents of all amphiboles were estimated using an empirical relation between the value of Fe^{3+}/Fe_{Total} and the OH content in mantle amphiboles (Popp et al., 1995a; King et al., 1999; Lamb & Popp, 2009). Given these values for Fe^{3+}/Fe_{Total} and OH, it is possible to determine the A-site occupancy by requiring the resulting formula to charge balance (Lamb & Popp, 2009). Amphiboles in these samples often occur rimming spinel and, in rare cases, pyroxene grains, indicating that, in most of these samples, the amphibole growth occurred after pyroxene and spinel. We infer, therefore, that the amphiboles are in equilibrium with the rims of chemically zoned pyroxenes and spinels, and, therefore, the rim compositions were used when mineral equilibria were applied to estimate P, T, aH_2O, fO_2 and fH_2.

Sample Description and Mineralogy

Eleven amphibole-bearing mantle xenoliths from the Southwestern U.S.A have been analyzed as part of this study. Eight samples are from the Grand Canyon. Two samples are from

Dish Hill, California and the one remaining sample is from Kilbourne Hole, New Mexico (Figure 2). All eleven samples contain co-existing olivine, orthopyroxene, clinopyroxene, amphibole and spinel (Figure 3a-d). Sample X174, from the Grand Canyon, also contains garnet.

Grand Canyon

Eight samples from the western Grand Canyon region of northwestern Arizona (X174, X192, X229, X286, X297, X299, X319) were analyzed. These samples were provided by Myron Best, and more detailed information on this location and a description of various xenoliths from this area may be found in Best (1970; 1975). Sample TF6 from Toroweap Valley was provided by J.C.A Riter and information on this location may be found in Riter (1999).

All eight of the Grand Canyon samples are amphibole-rich, with samples X192 and X286 containing as much as 50% amphibole. Amphibole occurs in varying amounts in these samples and exhibit three textural relations: disseminated grains, grains rimming spinel, and poikilitic. Samples X192 and X286 are dominated by a large poikilitic amphibole. The rest of the assemblage (ol, sp, opx, cpx) in these two samples, occurs as inclusions within the poikilitic amphibole (Figure 3a). Poikilitic amphibole also occurs in samples X229, X297 and X319; however, these samples contain < 50 % amphibole. Samples X229, X297, and X299 contain approximately 30% amphibole, while samples X174, X319 and TF6 are the least amphibole-rich, containing approximately ≤ 20%. All of these samples typically contain more than 30% olivine and less than 20% spinel. They also contain abundant (≤ 30%) pyroxenes, generally with a higher percentage of clinopyroxene as compared to orthopyroxene. Sample X174 contains abundant orthopyroxene, with only minor amounts of clinopyroxene (Figure 3b). In all of the samples, spinel is found both as individual grains and as grains rimmed by amphibole (Figure 3). Rock names, based on the relative proportions of ol, opx, and cpx are listed in Table 1 of the electronic Supplement.

Sample X174 contains both garnet and spinel, with a significant amount of spinel (≈ 20%) and lesser amounts of garnet (≈ 5%). The compositions of the garnets in sample X174 are homogenous with little or no core to rim variations in chemical composition (see Table 6 in the appendix). The garnets in this sample are rimmed by kelyphite (Figure 3b).

The olivines, amphibole, and spinels in all samples are chemically homogeneous (Tables 1, 2, and 5) as are many of the clinopyroxenes and orthopyroxenes (Tables 3 and 4). However, pyroxenes from samples X192, X297, X286 and X299 exhibit small core to rim chemical variations with a broad homogenous core and an Al-depleted, Si-rich rim (Figure 4a). Spinels from the Grand Canyon samples are Cr-poor and Al-rich, with Cr numbers (Cr# = Cr/Cr + Al) ranging from 0.002 to 0.077, and typically exhibit little if any chemical heterogeneity (Table 5). The olivines from these eight samples have Mg# (Mg# =Mg/(Mg + Fe)) that range from 0.77 to 0.90, and some of these samples, X174 for example, with the most Fe-rich olivines and Al-rich spinels (see below) are interpreted to be mantle cumulates (Best, 1975). In these cases, the estimation of values of aH_2O can provide information concerning the nature of the melts that crystallized the amphiboles and, therefore, may yield insight into mantle melt H_2O contents and metasomatism.

Dish Hill, California

Two samples from Dish Hill, California (Ba-1-72 and Ba2-1-1) have been provided by the Smithsonian Institution (these samples can also be identified using numbers provided by the Smithsonian, as listed in the electronic supplement). This location has been described by Wilshire and Trask (1971) and Luffi et al. (2009). Ba-1-72, for example, has been described by Wilshire et al. (1971; 1980). A portion (≈1/4) of the thin section from this sample consists solely of amphibole, presumably part of an amphibole-rich vein. The amphibole in the remainder of the Ba-1-72 is typically found rimming grains of spinel, but also occur as disseminated grains (Figure 3d). The

composition of the amphibole in the vein differs slightly from the amphibole found surrounding the spinels, and the disseminated amphibole grains are chemically homogenous (Table 2). Amphibole in sample Ba2-1-1 also occurs as both disseminated grains and as grains rimming spinel. Unlike many of the Grand Canyon samples, these two samples are not amphibole rich, as both contain less than 10% amphibole and they also do not contain any poikilitic amphibole. They contain abundant, compositionally homogeneous olivine (≥ 40%), pyroxene (≤ 30%) and Al-rich spinel (≤ 20%) (Tables 1, 4, 5). The olivine Mg# for samples Ba-1-72 and Ba2-1-1 are 0.88 and 0.90, respectively. Clinopyroxene grains exhibit subtle chemical zonation with a drop in Al content and an increase in Si contents from the core to the rim of a grain (Table 3). Samples from this locality are typically spinel peridotite xenoliths which may record evidence of metasomatic processes in the mantle (Wilshire et al., 1980; Luffi et al., 2009).

Kilbourne Hole, New Mexico

One xenolith, EP-3-84, from Kilbourne Hole, New Mexico has also been analyzed as part of this study (sample provided by the Smithsonian Institute). Information about the sample location and mineralogy of similar spinel-bearing xenoliths found in this location can be found in various publications (e.g., Irving, 1980; Perkins & Anthony, 2011; Satsukawa et al., 2011).

Sample EP-3-84 is clinopyroxene-rich (≈ 40%), with abundant spinel (≈ 30%) and olivine (≈15%) and lesser amounts of orthopyroxene (≈10%) and amphibole (≈ 5%). The olivine, amphibole, orthopyroxene, and spinel are all chemically homogeneous from core-to-rim (Tables 1, 2, 4, and 5). The clinopyroxene from this sample exhibits minor chemical zonation with a general decrease in Al content and an increase in Si contents from the core to the rim of a grain (Table 3 and Figure 4b). The Mg# for the olivine in this sample is 0.87. Samples from this locality have been interpreted in different ways. The clinopyroxene-rich samples, first described by Irving

(1980), were interpreted as pyroxene-rich xenoliths with a cumulate origin. However, those samples were clinopyroxenites and typically contained more clinopyroxene than sample EP-3-84. Peridotite xenoliths also occur at Kilbourne Hole (Perkins & Anthony, 2011; Satsukawa et al., 2011), and they contain minerals with compositions similar to those in EP-3-84, suggesting that this sample is not a cumulate. However, this conclusion does not rule out the possibility that the sample has interacted with metasomatic fluids, perhaps resulting in changes in mineralogy.

Estimation of Pressure and Temperature

Estimating values of aH_2O, fO_2 and fH_2 using mineral equilibria require an independent determination of the pressure (P) and temperature (T) of mineral equilibration. Pyroxene geothermometry was applied to determine temperature for all samples, whereas limiting values of P were estimated using multiple approaches discussed below.

Temperature

Geothermometers based on the compositions of co-existing pyroxenes have been widely applied in mantle rock (e.g., Nimis & Grütter, 2010). However, a number of different versions of the two-pyroxene geothermometer have been formulated (Wells, 1977; Bertrand & Mercier, 1985; Brey & Köhler, 1990; Taylor, 1998) and the accuracy of temperature estimates depends, in part, in choosing the most appropriate geothermometer. Nimis and Grütter (2010) prefer the two pyroxene geothermometer of Taylor (1998) (T98), as compared to other geothermometers that may be applied to mantle peridotites, in part because T98 more accurately reproduces temperatures of experiments designed to yield equilibrium compositions of co-existing pyroxenes. Two formulations of the two-pyroxene geothermometer, (1) the enstatite-in-Cpx thermometer of Nimis and Taylor (2000) (NT), and (2) the Ca-in-opx thermometer (Brey & Köhler, 1990) as modified by Nimis and Grütter (2010) (BKNG) agree with T98 within ± 30˚C and ±70˚C, respectively, over

the temperature range of 900 to 1200˚C (Nimis & Grütter, 2010). Thus, we have compared the results of three geothermometers (T98, NT, BKNG) in an effort to determine if a reliable estimate of the temperature of pyroxene equilibration had been determined (Table 6).

In some cases, accurate temperature estimates from conventional thermobarometry may require determining values of Fe^{3+}/Fe_{Total} in Fe-bearing minerals, including pyroxenes (Schumacher, 1991; Matjuschkin et al., 2014). The sensitivity of our temperature estimates to differences in Fe^{3+}/Fe_{Total} was evaluated by determining two pyroxene temperatures using two methods, described previously (charge balance and total Fe is Fe^{2+}), to determine values of Fe^{3+}/Fe_{Total} in pyroxenes. The maximum difference in temperature calculated using these methods is 20˚C. This small T difference is similar to other results indicating that the two-pyroxene thermometer, as applied to mantle rocks, is relatively insensitive to uncertainties in Fe^{3+}/Fe_{Total} (Brey & Köhler, 1990; Schumacher, 1991; Canil & O'Neill, 1996; Taylor, 1998).

Pressure

For spinel-bearing peridotites, the determination of pressure is challenging largely because equilibria between the major components of these rocks are generally not pressure sensitive (Köhler & Brey, 1990). For example, Köhler & Brey (1990) developed a geobarometer based on the exchange of Ca- between olivine and clinopyroxene, however, application of this geobarometer is limited by its sensitivity to temperature (O'Reilly et al., 1997; Smith, 1999) and any difficulties involved in the quantification of trace quantities of Ca in olivine.

The stability of spinel in mantle peridotites can be used to place limits on the pressure of mineral equilibration at a given temperature. Spinel stability in ultramafic rocks containing olivine, orthopyroxene, clinopyroxene, and spinel is limited by the formation of plagioclase at relatively low P, and by the formation of garnet at relatively high P. For many mantle peridotites,

the stability of spinel is restricted to between approximately 1 and 2 GPa, and, therefore, 1.5 GPa is sometimes inferred to be the P of mineral equilibration (O'Neill, 1981; Gasparik & Newton, 1984; Su et al., 2010). Xenoliths that originate from below the Moho may differ in mineralogy and mineral chemistry from typical mantle lherzolites and harzburgites. This includes certain samples examined in the study, as described previously, and differences in mineral chemistry have implications for the P-T limits of spinel stability. Thus, it is appropriate to evaluate the effects of mineral chemistry on the stability of spinel before estimating pressure of mineral equilibration (e.g., 1.5 GPa) based on the presence of this mineral.

Samples with mineral chemistries that differ from common mantle peridotites include those with sample numbers beginning with "X". The olivines in these samples have Mg numbers (Mg# = Mg/Mg+Fe) that range from 0.77 to 0.84 (Table 1) and, therefore, are relatively Fe-rich as compared to olivines from mantle peridotites. The spinels from these samples are Al-rich and Cr-poor with Cr# of 0.002 to 0.077 (Table 5). Cr extends the stability of spinel relative to plagioclase at low P (and garnet at high P). Thus, the range of spinel stability in samples with Al-rich spinels is not expanded relative to rocks containing spinels with higher Cr contents (e.g., Ba-1-72, Ba2-1-1, and TF6, Table 5), and estimates of the minimum pressure of spinel stability in the samples with Al-rich spinels, using the approach described in Lamb & Popp (2009), indicate minimum pressures of approximately 0.9 to 1.0 GPa.

In some cases, a geotherm for a particular location on earth has been inferred from garnet-bearing xenoliths that permit determination of both P and T from a single rock. If garnet-free xenoliths equilibrated along this same geotherm then the pressure of mineral equilibration may be determined given the temperature of mineral equilibration which is typically estimated from conventional geothermometry (O'Reilly & Griffin, 1985; Xu et al., 1996). To our knowledge, no

geothermal gradient, based on P-T estimates of xenoliths from the SW USA region, has been published. Therefore, we combined a heat flow value for the Grand Canyon of approximately 83 mW/m^2 (Blackwell & Richards, 2004) with the continental heat flow model of Pollack & Sass (1988) to determine a geothermal gradient for this region. Given the temperature of mineral equilibration estimated from two-pyroxene geothermoemtry (Table 6), this geotherm yields presures of approixmatley 1.4 to 1.6 GPa for the samples from the Grand Canyon. Many of these Grand Canyon xenoliths have been interpreted to be cumulates (Best, 1975), and the temperatures estimated from the compositions of co-existing pyroxenes may reflect igneous crystallization rather than equilibration along the geotherm. These pressure estimates may, therefore, be unreliable. They are, however, consistent with the stability of spinel in these samples and support the use of 1.5 GPa as a reasonable pressure estimate.

Sample X174 contains garnet, and the garnet-orthopyroxene barometer of Nickel & Green (1985) yields a pressure estimate of 1.1 GPa for this sample (choice of barometer is based on the work of Nimis & Grütter, 2010). Typically, garnet-bearing samples from the mantle are stable at higher pressures than those that contain spinel. However, the relative stability of these two phases, garnet and spinel, depends upon the chemistry of the bulk rock, as well as the pressure and temperature condtions. The chemical compostions of minerals in Sample X174 differs from all other samples as it contains the most Fe-rich olvine (Mg# = 0.77, Table 1), and a very Al-rich spinel (Cr/(Cr+Al) = 0.001, Table 5). The presence of garnet in this xenolith (X174), as compared to the other samples from the Grand Canyon, is likely a result of these differences in compostion, rather than differences in pressure. Although there is no guarantee that all xenoliths equlibrated at this pressure of 1.1 GPa all these samples , with the exception of TF6, are from the Western Grand Canyon and have very similar textures and minerals chemistries. Thus, we regard 1.1 GPa as the

best P estimate for samples from the Grand Canyon, a value that is only 0.1 to 0.2 GPa above the minimum pressure estimate for these samples.

A number of xenoliths from Kilbourne Hole equilibrated at pressures of approximately 1.1 to 1.3 GPa (Perkins & Anthony, 2011). We, therefore, suggest that a pressure that is similar to that chosen for the Grand Canyon samples,1.1 GPa, may be appropriate for sample EP-3-84.

Given the difficulty involved in determining a single value of pressure for spinel-bearing peridotites we have chosen to estimate values of fO_2, fH_2, and aH_2O at two different pressures. We used 1.5 GPa as one pressure estimate for these samples, consistent with certain previous studies (see above). The second pressure estimate is 1.1 GPa (based on sample X174, which contains garnet, see above). If 1.1 GPa is the best P estimate for samples from the Grand Canyon, then it could be argued that this P estimate should be reserved for those those samples, while a P estimate of 1.5 GPa could be applied to other samples from different locations or different mineral chemistries. However, given that these P estimates are associated with signficant uncertainty (1.5 GPa in particular) we have used both pressure estimates for all samples. It is important to note that the values of aH_2O, fO_2 and fH_2 estimated using mineral equilibria are not strongly P-dependent, such that change the value of P by ± 0.4 GPa has a very small effect, for example, on the estimated value of aH_2O (as discussed in subsequent sections of this paper).

Taylor's (1998) two-pyroxene thermometer yields temperatures from 880˚C to 980˚C at 1.5 GPa for the 11 xenoliths included in this study (Table 6). The temperatures recorded using the lower pressure estimate of 1.1 GPa, are generally 10 to 20˚ C lower than those estimated at 1.5 GPa (Table 6). At 1.5 GPa, the absolute temperature difference between the formulations of T98 and NT generally ranges from 0 to 30˚C, and the difference between T98 and BKNG ranges from 0 to 70˚C with and average difference of 47˚C. These differences are relatively small (see previous

discussion, and Nimis & Grütter (2010)) and the agreement between the three formulations of the two-pyroxene thermometer indicates that the co-existing pyroxenes equilibrated at these temperatures (Table 6).

RESULTS: ACTIVITIES OF FLUID SPECIES

Values of aH_2O estimated using Amphibole Dehydration Equilibria

A number of different H_2O-buffering equilibria involving the minerals in our samples can be written. The accuracy of the resulting estimate of aH_2O using any one of these equilibria will depend on various factors, including the accuracy of: (1) the P-T estimates, (2) the characterization of mineral chemistry, and (3) the models that describe the activity-composition (a-X) relations in various minerals. Not all activity models may be equally suitable given the mineral chemistry of our samples and the choice of activity model will, to some extent, dictate which H_2O-buffering equilibria will provide the most accurate estimate of aH_2O.

Lamb & Popp (2009) and Popp et al. (2006) have applied dehydration equilibria to estimate values of aH_2O in mantle rocks and have considered a number of different H_2O-buffering reactions as well as various models that describe the activity-composition relations in the minerals included in those reactions. For this study, we have adopted their approach and, therefore, estimates of aH_2O are based on the equilibria:

$$2\text{Pargasite} + \text{Enstatite} = 2\text{Forsterite} + 4\text{Diopside} + 2\text{Jadeite} + 2\text{Spinel} + H_2O \quad (1)$$

This equilibria was chosen largely because of the Mg-rich nature of olivine, orthopyroxene, and spinel, and the pargasite-rich amphibole found in these samples (Lamb & Popp, 2009).

THERMOCALC, a thermodynamic calculation program with self-consistent thermodynamic database (Powell et al., 1998), was chosen to estimate values of aH_2O based on equilibrium 1 (Lamb & Popp, 2009) largely because of the availability of relatively sophisticated

models describing the activity-composition (a-X) relations in amphiboles (Dale et al., 2005; Diener et al., 2007; Diener & Powell, 2012). The method described in Lamb & Popp (2009) used a combination of activity models consistent with either the THERMOCALC and MELTS software packages to determine values of aH_2O using equilibrium 1 (Ghiorso & Sack, 1995; Asimow & Ghiorso, 1998; Powell et al., 1998). This choice was based on the argument that the activity models developed for MELTS are designed to be applicable to mantle compositions and/or conditions whereas when Lamb and Popp (2009) was published some THERMOCALC activity models e.g., spinel) were developed for application to crustal compositions and conditions. Thus, the activities of olivine, spinel, and pyroxenes were determined using models designed for MELTS (Sack & Ghiorso, 1989; 1991, 1994 a,b), while the activity of amphibole was determined using the THERMOCALC model of Dale et al. (2005). However, Lamb & Popp (2009) demonstrated that the choice of activity model, whether developed for MELTS or for THERMOCALC, has little effect on the calculated end-member activities for mantle Mg_2SiO_4 in olivine, $Mg_2Si_2O_6$ in orthopyroxene, and $CaMgSi_2O_6$ and $NaAlSi_2O_6$ in clinopyroxene. Because of the Mg-rich nature of many of these minerals, specifically olivine, orthopyroxene and clinopyroxene, the non-ideal activities of these end-members are also very similar to ideal activities over this PT range.

However, subsequent to the publication of Lamb & Popp (2009), activity models consistent with THEREMOCALC have been developed and some of these models are specifically applicable to mantle compositions and/or conditions (Jennings & Holland, 2015; Green et al., 2016). For example, the new Cr-bearing spinel model considers components common to mantle spinels that the older spinel model of White et al. (2002), which was originally developed for magnetite, ignored (e.g., Cr).

This study has estimated values of aH_2O with dehydration equilibria using two different methods in an effort to determine if the most recently published activity models yield values of aH_2O that are significantly different than those estimated previously (Lamb & Popp, 2009). The first method, hereafter referred to as Method A, estimates values of aH_2O using the combination of MELTS and THERMOCALC models as described in Lamb & Popp (2009). The second method, hereafter referred to as Method B, estimates values of aH_2O using the mantle mineral models (Jennings & Holland, 2015) and new amphibole model of Green et al. (2016). For each of these methods, the values of aH_2O will be estimated using dehydration equilibria at 1.1 and 1.5 GPa (Table 7).

Application of equilibrium (1) yields values of aH_2O that are less than 0.30 for all of the mantle xenoliths in this study (Table 7) regardless of which method is used. At 1.5 GPa, the values estimated using Method A, range from 0.03 to 0.12, while those estimated using Method B, range from 0.05 to 0.26. We consider these values to be relatively small, or low, such that if a grain boundary fluid were present at the time of mineral equilibration this fluid could not be dominated by H_2O. However, it would be incorrect to simply assume a fluid phase at lithostatic pressure is present because fluid-absence is possible (Kang et al., 2017).

The average difference in values of aH_2O estimated using the two methods is 0.05. In general, values of aH_2O estimated using Method B are greater than those estimated using Method A, even though all of these values are still relatively small. Further, given that all values of aH_2O estimated using Method A or Method B are consistently low, this would further suggest that future estimations of aH_2O using THERMOCALC, can be successfully estimated using either of the two methods described in this paper.

A pressure uncertainty of ± 0.4 GPa yields a difference of ± 0.04 in values of aH_2O, while a temperature change of ± 50 ˚C yields a similar change in estimated values of aH_2O (± 0.04). Therefore, given the combined uncertainties involved in P, T and activity models, the overall uncertainty for values of aH_2O is likely better than ± 0.1.

Estimations of Oxygen Fugacity

In the upper mantle, values of fO_2 may be affected by several factors, including bulk composition, tectonic setting, and fluids (Wood, 1990; Wood et al., 1990; Woodland et al., 1992; Woodland & Koch, 2003; Frost & McCammon, 2008). Values of fO_2 are typically reported relative to an oxygen-buffering equilibrium, such as the Fayalite-Magnetite-Quartz (FMQ) buffer, which is based on the equilibria:

$$3Fe_2SiO_4 + O_2 = 2Fe_3O_4 + 3SiO_2 \quad (2)$$

and typical values of fO_2 for peridotites the uppermost mantle range from Δlog FMQ-3 to Δlog FMQ+2 (Wood, 1990; Woodland et al., 1992; Woodland & Koch, 2003; Miller et al., 2016). In general, the mantle beneath ancient cratons records relatively reducing values of $fO2$, with Δlog FMQ typically from -2.5 to 0.5, while non-cratonic are typically more oxidizing, with Δlog FMQ from -1 to 2.5 (Wood & Virgo, 1989a; Wood et al., 1990; Brandon & Draper, 1996; Woodland & Koch, 2003).

Values of fO_2 have been estimated for mantle xenoliths that contain co-existing spinel, olivine and orthopyroxene, using the equilibria:

$$6Fe_2SiO_4 + O_2 = 3Fe_2Si_2O_6 + 2Fe_3O_4 \quad (3)$$

and in this study, we applied the calibration of Wood (1990):

$$\Delta\log fO_2(\mathrm{FMQ}) = 0.35 + \frac{220}{\mathrm{T}} - \frac{0.0369\mathrm{P}}{\mathrm{T}} - 12\log(X_{Fe}^{ol})$$

This is a preprint, the final version is subject to change, of the American Mineralogist (MSA)
Cite as Authors (Year) Title. American Mineralogist, in press.
DOI: https://doi.org/10.2138/am-2019-6602

$$-\frac{2620\,(X_{Mg}^{ol})^2}{T} + 3\log\,(X_{Fe}^{M1}X_{Fe}^{M2})^{opx} + \ 2\log\,(a_{Fe_3O_4}^{sp}) \qquad (4)$$

For this reaction, the P is in bars, T in in K, (X_{Fe}^{ol}) and (X_{Mg}^{ol}) are the mole fractions of Mg and Fe end-members in olivine, $(X_{Fe}^{M1}X_{Fe}^{M2})^{opx}$ are the atomic fraction of Fe in both the M1 and M2 sites in orthopyroxene (based upon charge balance), and $a_{Fe_3O_4}^{sp}$ is the activity of Fe_3O_4 in spinel. The estimated values of fO_2 using the oxybarometer of Wood (1990) for our samples at 1.5 GPa range from Δlog FMQ -0.8 to Δlog FMQ +0.5 (Table 8). Values of fO_2 have also been determined using the spinel oxybarometer of Miller et al. (2016), and these values range from ΔlogFMQ -0.5 to Δlog FMQ +0.6 (Table 8). Uncertainties determined for these values of fO_2, estimated using Miller et al. (2016), typically range from ± 0.31 to ± 0.55 log units. However, the uncertainties for samples X192, EP-3-84, and Ba-1-72 are significantly larger, with values of ±0.8, ±0.9, and ±1.5, respectively.

Differences between values of fO_2 estimated using Miller et al. (2016), and those estimated using the calibration of Wood (1990), are generally not large (often < 0.3 log units, Table 8), and in most samples (8 of 11) the fO_2 values estimated using Miller et al. (2016) are more oxidizing than those estimated using Wood (1990). This finding seems inconsistent with the results of Miller et al. (2016) who found that values of fO_2 estimated using their calibration are generally more reduced than those estimated with earlier calibrations. This discrepancy may be explained by differences in the sensitivity of each calibration to the amount of Fe^{3+} in the opx.

Values of fO_2 based on Wood (1990) (ΔlogFMQ -1 to ΔlogFMQ +0.5 at 1.5 GPa) were determined using amounts of Fe^{3+} in the opx that were estimated using charge balance (see the previous discussion). However, when all Fe is considered as Fe^{2+}, the resulting values of fO_2 become more oxidizing (ΔlogFMQ -0.2 to Δlog FMQ +1.0). This change to more reducing values of fO_2 with increasing values of Fe^{3+}/Fe_{Total} in the opx may seem counter-intuitive. However,

reduction of Fe^{2+} through the creation of Fe^{3+} reduces the activity of $Fe_2Si_2O_6$ in equilibrium (3) which must result in smaller values of fO_2 as estimated with equation (4).

Miller et al. (2016) also estimates values of fO_2 using equation (3), but they apply two additional equilibria and the final result is, therefore, based on three different oxygen-buffering equilibria. Values of fO_2 inferred using the other two equilibria (not equation 3) are less sensitive to the amount of Fe^{3+} in the orthopyroxene as compared to values estimated using equilibrium 3. Thus, additional Fe^{3+} in the opx does not yield the same reduction in the value of fO_2 when all three equilibria are considered as opposed to estimating fO_2 using equilibrium (3). However, increasing amounts of Fe^{3+} also yields increasingly large discrepancies between the three values of fO_2 as estimated using the three equilibria applied by Miller et al. (2016). This suggests that the effect of significant amounts of Fe^{3+} in opx on estimated values of fO_2 are not completely understood. Thus, while increasing amounts of Fe^{3+} in the opx is associated with more reduced values of fO_2, it may also be associated with greater uncertainties in values of fO_2 estimated using mineral equilibria.

Estimations of fH_2 using Amphibole Dehydrogenation Equilibria

Values of hydrogen fugacity (fH_2) can be estimated at any given value of P and T, from the chemical composition of a mantle amphibole, including the Fe^{2+} and Fe^{3+} content (Popp & Phillips, 1995; Popp et al., 2006). This approach is based on the Fe-amphibole end-member reaction:

$$Ca_2Fe_5^{2+}Si_8O_{22}(OH)_2 = Ca_2Fe_3^{2+}Fe_2^{3+}Si_8O_{24} + H_2 \quad (5)$$

with the equilibrium constant (K) defined as:

$$K = fH_2\ (28.94)\frac{(XFe^{3+})^2(X_{\square})^2}{(XFe^{2+})^2(X_{OH})^2} * \phi = K_x * \phi \quad (6)$$

for which

$$\log \mathrm{K}_x = 4.23 - \frac{4380}{T} + \{1.37 \times [(\mathrm{Ti} + \mathrm{Al_{total}}) - 2.49]\} + \left\{\frac{88}{T}[\mathrm{P} - 1(\mathrm{kbar})]\right\} \quad (7)$$

where □= H-vacancy on the O3 anion position, ϕ is the activity coefficient term and K_x represents the thermodynamic mole fraction term, and T is temperature in K (Popp et al., 2006). Values of Fe^{3+}/Fe_{Total} for the amphibole from all the samples, except Ba2-1-1 and TF6, have been estimated using the methods of Lamb et al. (2012) (see Analytical Methods section above and Table 2).

Values of fH_2 have been determined for nine samples at 1.5 GPa and these range from 6 to 91 bars, or log fH_2 of 0.8 to 2.0 ± 0.3 (Table 8). Given a value of fH_2 from the dehydrogenation equilibria, and a value of fO_2 estimated using the Miller et al. (2016) oxybarometer, it is possible to estimate a value of fH_2O using the equilibria $2H_2 + O_2 = 2H_2O$ where the products and reactants are related by the equilibrium constant (K_{H_2O}) as follows:

$$K_{H_2O} = \frac{f_{H_2}(f_{O_2})^{1/2}}{f_{H_2O}} \quad (8)$$

For 8 of the mantle xenoliths where the Fe^{3+}/Fe_{Total} have been estimated, this method yields low values of aH_2O (where $aH_2O = fH_2O/fH_2O^{\circ}$ and fH_2O is the fugacity of pure H_2O at the P and T of interest) that are less than to 0.20 (Table 8). The 8th sample, Ba-1-72, yields an anomalously high value of aH_2O of 0.57 (Table 8). This value is much greater than the value of aH_2O (0.11), estimated using this method but with fO_2 estimated using the oxybarometer of Wood (1990). The opx in sample Ba-1-72 has an unusually elevated value of Fe^{3+}/Fe_{Total} which results in a relatively reducing value of fO_2 when the Wood oxybarometer is applied, but this is not the case when the Miller et al oxybarometer is applied (see the previous discussion and Table 8). It may be notable that the more reducing value of fO_2 estimated for sample Ba-1-72 using the Wood oxybarometer, when combined with our estimate of fH_2, yields a low value of aH_2O consistent with those recorded in other samples.

This is a preprint, the final version is subject to change, of the American Mineralogist (MSA)
Cite as Authors (Year) Title. American Mineralogist, in press.
DOI: https://doi.org/10.2138/am-2019-6602

DISCUSSION

For any one sample, the value of aH_2O estimated using amphibole dehydration equilibria (Table 7) should be equivalent to the value of aH_2O estimated using the combination of amphibole dehydrogenation equilibria and oxybarometry (hereafter referred to as the combined approach). For the nine samples, in which both methods (dehydration equilibria and the combined approach) could be used to estimate values of the aH_2O, the average difference between these two values of aH_2O is 0.04 (Figure 6), with the largest difference (0.45) observed in sample Ba-1-72 (see discussion above regarding sample Ba-1-72). This good agreement indicates that these samples from the SW U.S.A, all equilibrated at values of $aH_2O < 0.20$. These values of aH_2O demonstrate that the presence of amphibole does not require H_2O-rich conditions, a result that agrees with previous studies (Lamb & Popp, 2009; Bonadiman et al., 2014; Kang et al., 2017). This result may seem counter-intuitive (e.g., Marshall et al., 2018), and indicates the presence of amphibole depends, at least in part, upon factors other than aH_2O, and these factors may include K, Na, and/or Ti contents that are elevated as compared to amphibole-free mantle (Mandler & Grove, 2016).

It has been argued that amphiboles may not be good indicators of mantle fluids due to possible diffusive H-loss during emplacement on Earth's surface (Dyar et al., 1993). However, the comparison of values of aH_2O for any given sample, as determined using dehydration equilibria and the combined approach, can serve as a test of the H-retention of mantle amphiboles. This test is possible largely because values of aH_2O estimated using the combined approach are more sensitive to H-loss from amphibole than those estimated using dehydration equilibria (Lamb & Popp, 2009). This difference in sensitivity is illustrated in Figure 7, which was constructed by estimating values of aH_2O for sample X297 over a range of amphibole H-contents all greater than

the estimated H-content (1.43 atoms per formula unit (apfu) in sample X297). Thus, Figure 7, plots values of aH_2O as a function of the H-content of the amphibole. Sample X297 records low values of aH_2O using either the combined approach or dehydration equilibria (black circles on Figure 7). Adding H to the amphibole should increase the value of aH_2O for both methods and would better reflect true mantle values if retrograde amphibole H-loss had occurred. In this case increasing the H-content of the amphibole should yield a H-content closer to the equilibrium mantle values and, therefore, should improve the agreement between the estimated using the two approaches (combined vs. dehydration). As expected, adding H to the amphibole formula does increase the estimated value of aH_2O using either method, as illustrated by the two curves in Figure 7. The resulting values of aH_2O, however, begin to diverge significantly once more than approximately 0.04 H apfu is added to the amphibole. Figure 7 shows that increasing amphibole H-contents produces small changes in aH_2O estimated using dehydration equilibration as compared to much larger increases in values of aH_2O estimated using the combined approach. These results indicate that the amphibole in sample X297 did not suffer loss of H in amounts more than approximately 0.04 H apfu. All other samples from this study yield similar results and, therefore, H-loss from these amphiboles was limited, and the overall agreement between values of aH_2O estimated using both methods indicates that the amphiboles in these samples have retained their mantle H-contents.

Values of mantle aH_2O, fO_2 and the Presence of Oxy-Amphiboles

Amphibole-bearing sub-continental xenoliths may be relatively oxidized when compared to spinel peridotites that do not contain amphibole but are also sub-continental. For example, Bryndzia & Wood (1990) report values of $\Delta\log fO_2$(FMQ) for amphibole-bearing samples that range from approximately 0 to +1.5, which is within the range of samples with no amphibole

($\Delta\log fO_2$(FMQ) from -1.5 to 2.), but are relatively oxidizing on average. However, values of $\Delta\log fO_2$ recorded by the samples in this study range from FMQ-1 to FMQ+0.5 (Table 8), and these values of $\Delta\log fO_2$ are not particularly oxidizing compared to the range typical of the upper mantle (FMQ-3 to FMQ+2) (Wood, 1990; Woodland et al., 1992; Woodland & Koch, 2003) and fall within the range of mantle peridotites from non-cratonic settings (Wood et al., 1990; Brandon & Draper, 1996).

Metasomatism of spinel peridotite xenoliths from Dish Hill (including Ba-2-1) resulted in an increase in the Fe-content and Fe^{3+}/Fe_{Total} of these rocks, as well as the production of amphibole with 0.70 to 0.84 Fe^{3+}/Fe_{Total} (McGuire et al., 1991). These results were interpreted to indicate oxidation via metasomatism. The value of fO_2 for samples Ba-2-1 is, however, not unusually elevated (Table 8). Furthermore, values of hydrogen fugacity (fH_2) estimated for the amphiboles from these samples demonstrate that increased values of fO_2, while possible, are not required to explain the elevated values of Fe^{3+}/Fe_{Total} recorded in these peridotites (Popp et al., 1995b). Instead, low values of aH_2O could also explain the presence of oxy-amphiboles.

If elevated values of fO_2 are not required to stabilize amphiboles with a significant oxy-component, then there may be little or no correlation between values of oxygen fugacity and the presence of mantle amphiboles. This may be surprising given that experimental investigations of oxy-amphiboles have demonstrated that, at a given temperature, fluid pressure, and a fluid dominated by H_2O, the value of Fe^{3+}/Fe_{Total} in an amphibole of an otherwise fixed composition increases with increasing oxygen fugacity (Popp et al., 1995a; 2006). This result is predictable because these experiments were conducted in the presence of an H_2O rich fluid which means that the values of fH_2O is essentially fixed at high values. In this situation, and at some constant P and T, raising the value of fO_2 must result in lower values of fH_2 (see equilibria 8). If mantle

amphiboles equilibrated with an H_2O-rich fluid then the presence of amphiboles with a significant oxy-component should, therefore, indicate elevated values of mantle fO_2, particularly amphibole with significant Fe^{3+} contents. We have, therefore, plotted the ferric-ferrous ratios of amphibole vs. the value of oxygen fugacity for our samples, as well as samples described in previous studies (McGuire et al., 1991; Lamb & Popp, 2009; Bonadiman et al., 2014; Gentili et al., 2015). The results, shown in Figure 8, indicate that there is no significant correlation between values of $\Delta \log fO_2$ (FMQ) and the Fe^{3+}/Fe_{Total} ratio of the amphiboles. Furthermore, many of these fO_2 values (Figure 8) are relatively reducing (<FMQ).

This result, little or no correlation between values of fO_2 and the oxidation state of Fe in the amphiboles, is consistent with low values of aH_2O as estimated in this study. One possible mechanism to account for the values of fH_2O and fO_2 estimated in this study involves the production of amphibole in a system with limited amounts of H_2O or H (e.g., H may be contained within nominally anhydrous phases). In this case, the amphibole may consume much of the available H resulting in low values of aH_2O and an amphibole with significant oxy-amphibole component even if values of fO_2 are relatively reducing (Popp et al., 1995b; Kang et al., 2017).

Comparing Values of aH_2O with Predicted Olivine H_2O Contents

Values of aH_2O estimated in this study might be used to predict the amount of H_2O contained in nominally anhydrous phases from the mantle. However, a quantitative comparison is only possible if the relation between values of fH_2O and the H_2O content of any particular NAM has been determined experimentally ($aH_2O = fH_2O/f^oH_2O$; where f^oH_2O is the fugacity of pure H_2O at the P-T conditions of interest). This is possible for olivine given that experimental studies relating olivine H_2O contents to values of, P, T, and fH_2O (Mosenfelder et al., 2006). In addition to P, T, and fH_2O the concentration of H_2O in olivine may also be a function of Fe content (Zhao

et al., 2004), oxygen fugacity and possibly Ti and Al contents (Gaetani et al., 2014). The values of aH_2O estimated in this study (Table 8), in combination with T estimates at 1.5 GPa (Tables 7 and 8) and the calibrations of Zhao et al. (2004), Mosenfelder et al. (2006), and Gaetani et al. (2014) yield olivine H_2O contents that are less than 45 wt. ppm for all samples (Table 9). Not surprisingly, the samples with the highest values of aH_2O yield the highest olivine H_2O contents. In general, the predicted olivine H_2O contents estimated using Mosenfelder et al. (2006) are higher compared to those estimated with either Gaetani et al. (2014) and Zhao et al. (2004). However, all three calibrations yield relatively low values of olivine H_2O contents as compared to the total range of H_2O contents measured in olivines from mantle xenoliths (approximate range of 0 to 300 wt. ppm, Peslier, 2010; Peslier et al., 2017).

The estimates of the olivine H_2O contents presented in Table 9 permit a comparison with previously published determination of the H_2O contents of NAMs from Southwestern USA. Dixon et al. (2004), for example, argue that the low viscosities of the upper mantle beneath the western USA are the result of the combined effect of relatively high H_2O contents and elevated temperatures. These authors suggest olivine water concentrations of approximately 50 ppm or higher. Li et al. (2008) measured H_2O contents in nominally anhydrous minerals contained in peridotite xenoliths from the southwestern USA. For example, the measured H_2O contents for olivines from the Grand Canyon range from 12 to 30 ppm by weight (Li et al., 2008). In both of these studies the subducted Farallon plate is thought to be the source of H_2O that hydrated the upper mantle resulting in elevated H_2O contents.

Our predicted values of olivine H_2O contents (Table 9), based on the Gaetani et al. (2014), range from 6 to 17 wt. ppm (1.1 GPa) or 10 to 28 wt. ppm (1.5 GPa). At Dish Hill, the range of olivine H_2O contents for two samples measured by Li et al. (2008) are 11 and 13 weight ppm

which are identical to the values we predict at 1.1 GPa, but slightly smaller than the 18 and 19 wt. ppm predicted at 1.5 GPa (Table 9). Obviously, there is significant overlap in these values, and, given the uncertainties involved, it not clear that any significance may be attached to any differences in these values. However, it may be worth noting that many of the lowest values of olivine H_2O contents (predicted) are from Grand Canyon samples interpreted to be cumulates (Table 9).

Obviously, cumulates precipitate directly from magmas. In other cases, amphibole may be a product of mantle metasomatism, and the metasomatizing fluid may be a magma. Metasomatism typically involves the addition of various chemical components (e.g., Fe, Ti, alkali elements, or H_2O) and some of these may be required to stabilize amphiboles. It is possible, however, that addition of H_2O is not required, and as amphiboles nucleate and grow they may scavenge any H_2O present in the rock (e.g., in NAMs) and this process could produce values of aH_2O that are significantly less than 1. In this scenario, amphibole growth could lower the H_2O-contents of NAMs, and this process may have important implications for the rheology of an olivine-rich uppermost mantle. If the formation of amphibole results in H_2O-loss from NAMs then the strength of these NAMs will likely increase (Mei & Kohlstedt, 2000b). Thus, the formation of amphibole may actually serve to strengthen mantle rocks.

IMPLICATIONS

All the samples from the SW USA record values of aH_2O that are less than 0.3, as estimated using amphibole equilibria. For samples in which two values of aH_2O could be estimated using the two different approaches, these values agree within uncertainty. This suggests that the amphiboles in these samples have not undergone significant, if any, retrograde H-loss during

transport to the Earth's surface and that careful application of amphibole equilibria can reliably estimate values of aH_2O in samples from the Earth's mantle.

We consider these values of aH_2O to be low, such that a lithostatically-pressured fluid in equilibrium with these rocks at elevated P and T could not be H_2O-rich. Thus, this study demonstrates that the presence of amphibole does not require H_2O-rich conditions, a result consistent with previous studies of both crustal (Lamb & Valley, 1988) and mantle rocks (Lamb & Popp, 2009). Although values of aH_2O are significantly less than unity, predicted olivine H_2O contents (Table 9) are similar to those measured in olivines from the Colorado Plateau (Li et al., 2008). However, all values of olivine H_2O contents are smaller than 50 ppm, the value suggested by Dixon et al. (2004) based on the estimated viscosity of the mantle beneath the Colorado Plateau. It is possible, however, that the mantle beneath the Colorado Plateau is heterogeneous. The xenolith record indicates both a variety of rock types and variations in NAM H_2O contents (Best, 1970; Best, 1975; Riter, 1999; Li et al., 2008; Perkins & Anthony, 2011). Perhaps, then, strain is in mantle is not homogeneous, but localized and concentrated in weaker zones, and that these areas of relative weakness are sufficient to account for the relatively low viscosities beneath the Colorado Plateau. Zones where strain is concentrated may correspond to regions of elevated H_2O contents, however, other factors, such as the heterogeneous distribution of melt, could also serve to localize strain.

ACKNOWLEDGEMENTS

This paper has benefitted from comments provided by two anonymous reviewers. We would like to thank Myron Best and the Smithsonian Institute, specifically the Division of Petrology and Volcanology, Department of Mineral Sciences, for providing the xenolith samples used in this study. Thanks also to Ayati Ghosh for assistance in requesting samples, Robert Popp

for assistance and enlightening discussions, and, Ray Guillemette for his assistance with the electron microprobe analyses at Texas A&M. Support for this research was provided, in part, by a grant awarded to W. Lamb and R. Popp from the Texas Advanced Research Program.

REFERENCES

Albee, A.L., and Chodos, A.A. (1970) Semiquantitative Electron Microprobe Determination of Fe^{2+}/Fe^{3+} and Mn^{2+}/Mn^{3+} in Oxides and Silicates and Its Application to Petrologic Problems. American Mineralogist, 55, 491-501.

Asimow, P.D., and Ghiorso, M.S. (1998) Algorithmic modifications extending MELTS to calculate subsolidus phase relations. American Mineralogist, 83, 1127-1132.

Bali, E., Bolfan-Casanova, N., and Koga, K.T. (2008) Pressure and temperature dependence of H solubility in forsterite: An implication to water activity in the Earth interior. Earth and Planetary Science Letters, 268, 354-363.

Ballhaus, C., Berry, R., and Green, D. (1991) High pressure experimental calibration of the olivine-orthopyroxene-spinel oxygen geobarometer: implications for the oxidation state of the upper mantle. Contributions to Mineralogy and Petrology, 107, 27-40.

Bell, D.R., and Rossman, G.R. (1992) Water in earth's mantle- The role of nominally anhydrous minerals. Science, 255, 1391-1397.

Beran, A., and Libowitzky, E. (2006) Water in natural mantle minerals II: Olivine, garnet and accesssory minerals. In Keppler, H., and Smyth, J.R., Eds. Water in Nominally Anhydrous Minerals, 62, 155-167. Mineralogical Society of America.

Berry, A.J., O'Neill, H.S.C., Hermann, J., and Scott, D.R. (2007) The infrared signature of water associated with trivalent cations in olivine. Earth and Planetary Science Letters, 261, 134-142.

Bertrand, P., and Mercier, J.-C.C. (1985) The mutual solubility of coexisting ortho- and clinopyroxene: toward an absolute geothermometer for the natural system? Earth and Planetary Science Letters, 76, 109-122.

Best, M.G. (1970) Kaersutite-peridotite inclusions and kindred megacrysts in basanitic lavas, Grand Canyon, Arizona. Contributions to Mineralogy and Petrology, 27, 25-44.

Best, M.G. (1975) Amphibole-bearing cumulate inclusions, Grand Canyon, Arizona and their bearing on silica-undersaturated hydrous magmas in the upper mantle. Journal of Petrology, 16, 212-236.

Blackwell, D.D., and Richards, M.C. (2004) Geothermal Map of North America. AAPG.

Bolfan-Casanova, N. (2005) Water in the Earth's mantle. Mineralogical Magazine, 69, 229-258.

Bonadiman, C., Nazzareni, S., Coltorti, M., Comodi, P., Giuli, G., and Faccini, B. (2014) Crystal chemistry of amphiboles: implications for oxygen fugacity and water activity in lithospheric mantle beneath Victoria Land, Antarctica. Contributions to Mineralogy and Petrology, 167, 1-17.

Brandon, A.D., and Draper, D.S. (1996) Constraints on the origin of the oxidation state of mantle overlying subduction zones: An example from Simcoe, Washington, USA. Geochimica Et Cosmochimica Acta, 60, 1739-1749.

Brey, G.P., and Köhler, T. (1990) Geothermobarometry in Four-phase Lherzolites II. New Thermobarometers, and Practical Assessment of Existing Thermobarometers. Journal of Petrology, 31, 1353-1378.

Brown, G. (1980) Olivines and silicate spinels. Reviews in Mineralogy and Geochemistry, 5, 275-381.

Bryndzia, L.T., and Wood, B.J. (1990) Oxygen thermobarometry of abyssal spinel peridotites: the redox state and C–O–H volatile composition of the Earth's sub-oceanic upper mantle. American Journal of Science, 290, 1093-1116.

Canil, D., and O'Neill, H.S.C. (1996) Distribution of Ferric Iron in some Upper-Mantle Assemblages. Journal of Petrology, 37, 609-635.

Dale, J., Powell, R., White, R.W., Elmer, F.L., and Holland, T.J.B. (2005) A thermodynamic model for Ca–Na clinoamphiboles in Na_2O–CaO–FeO–MgO–Al_2O_3–SiO_2–H_2O–O for petrological calculations. Journal of Metamorphic Geology, 23, 771-791.

Davis, F.A., Cottrell, E., Birner, S.K., Warren, J.M., and Lopez, O.G. (2017) Revisiting the electron microprobe method of spinel-olivine-orthopyroxene oxybarometry applied to spinel peridotites. American Mineralogist, 102, 421-435.

Demouchy, S., Jacobsen, S.D., Gaillard, F., and Stern, C.R. (2006) Rapid magma ascent recorded by water diffusion profiles in mantle olivine. Geology, 34, 429-432.

Diener, J.F.A., and Powell, R. (2012) Revised activity–composition models for clinopyroxene and amphibole. Journal of Metamorphic Geology, 30, 131-142.

Diener, J.F.A., Powell, R., White, R.W., and Holland, T.J.B. (2007) A new thermodynamic model for clino- and orthoamphiboles in the system Na_2O–CaO–FeO–MgO–Al_2O_3–SiO_2–H_2O–O. Journal of Metamorphic Geology, 25, 631-656.

Dixon, J.E., Dixon, T.H., Bell, D.R., and Malservisi, R. (2004) Lateral variation in upper mantle viscosity: role of water. Earth and Planetary Science Letters, 222, 451-467.

Droop, G.T.R. (1987) A General Equation for Estimating Fe-3+ Concentrations in Ferromagnesian Silicates and Oxides from Microprobe Analyses, Using Stoichiometric Criteria. Mineralogical Magazine, 51, 431-435.

Dyar, M.D., McGuire, A.V., and Ziegler, R.D. (1989) Redox equilibria and crystal chemistry of coexisting minerals from spinel lherzolite mantle xenoliths. American Mineralogist, 74, 969-980.

Dyar, M.D., Mackwell, S.J., McGuire, A.V., Cross, L.R., and Robinson, J.D. (1993) Crystal chemistry of Fe^{3+} and H^{+} in mantle kaersutite-Implications for mantle metasomatism. American Mineralogist, 78, 968-979.

Fialin, M., Bezos, A., Wagner, C., Magnien, V., and Humler, E. (2004) Quantitative electron microprobe analysis of $Fe^{3+}/\Sigma Fe$: Basic concepts and experimental protocol for glasses. American Mineralogist, 89, 654-662.

Fialin, M., Wagner, C., Metrich, N., Humler, E., Galoisy, L., and Bezos, A. (2001) $Fe^{3+}/\Sigma Fe$ vs. Fe La peak energy for minerals and glasses: Recent advances with the electron microprobe. American Mineralogist, 86, 456-465.

French, B.M. (1966) Some Geological Implications of Equilibrium between Graphite and a C - H - O Gas Phase at High Temperatures and Pressures. Reviews of Geophysics, 4, 223-&.

Frost, D.J., and McCammon, C.A. (2008) The Redox State of Earth's Mantle. Annual Review of Earth and Planetary Sciences, 36, 389-420.

Gaetani, G.A., and Grove, T.L. (1998) The influence of water on melting of mantle peridotite. Contributions to Mineralogy and Petrology, 131, 323-346.

Gaetani, G.A., O'Leary, J.A., Koga, K.T., Hauri, E.H., Rose-Koga, E.F., and Monteleone, B.D. (2014) Hydration of mantle olivine under variable water and oxygen fugacity conditions. Contributions to Mineralogy and Petrology, 167, 1-14.

Gasparik, T., and Newton, R.C. (1984) The reversed alumina contents of orthopyroxene in equilibrium with spinel and forsterite in the system $MgO-Al_2O_3-SiO_2$. Contributions to Mineralogy and Petrology, 85, 186-196.

Gentili, S., Bonadiman, C., Biagioni, C., Comodi, P., Coltorti, M., Zucchini, A., and Ottolini, L. (2015) Oxo-amphiboles in mantle xenoliths: evidence for H2O-rich melt interacting with the lithospheric mantle of Harrow Peaks (Northern Victoria Land, Antarctica). Mineralogy and Petrology, 1-19.

Ghiorso, M., and Sack, R. (1995) Chemical mass transfer in magmatic processes IV. A revised and internally consistent thermodynamic model for the interpolation and extrapolation of

liquid-solid equilibria in magmatic systems at elevated temperatures and pressures. Contributions to Mineralogy and Petrology, 119, 197-212.

Grant, K.J., Brooker, R.A., Kohn, S.C., and Wood, B.J. (2007) The effect of oxygen fugacity on hydroxyl concentrations and speciation in olivine: Implications for water solubility in the upper mantle. Earth and Planetary Science Letters, 261, 217-229.

Green, D.H. (2015) Experimental petrology of peridotites, including effects of water and carbon on melting in the Earth's upper mantle. Physics and Chemistry of Minerals, 42, 95-122.

Green, D.H., and Falloon, T.J. (1998) Pyrolite: A Ringwood concept and its current expression. In Jackson, I., Ed. The Earth's Mantle: Composition, Structure, and Evolution, 311-380. Cambridge University Press, Cambridge.

Green, E.C.R., White, R.W., Diener, J.F.A., Powell, R., Holland, T.J.B., and Palin, R.M. (2016) Activity–composition relations for the calculation of partial melting equilibria in metabasic rocks. Journal of Metamorphic Geology, 34, 845-869.

Höfer, H.E., Brey, G.P., Schulz-Dobrick, B., and Oberhänsli, R. (1994) The Determination of the Oxidation-State of Iron by the Electron-Microprobe. European Journal of Mineralogy, 6, 407-418.

Ingrin, J. (2006) Diffusion of hydrogen in minerals. Reviews in Mineralogy and Geochemistry, 62, 291.

Ingrin, J., and Skogby, H. (2000) Hydrogen in nominally anhydrous upper-mantle minerals concentration levels and implications. European Journal of Mineralogy, 12, 543-570.

Ingrin, J., Hercule, S., and Charton, T. (1995) Diffusion of hydrogen in diopside: Results of dehydration experiments. Journal of Geophysical Research, 100, 15489-15499.

Ionov, D.A., and Wood, B.J. (1992) The oxidation state of subcontinental mantle: oxygen thermobarometry of mantle xenoliths from central Asia. Contributions to Mineralogy and Petrology, 111, 179-193.

Irving, A.J. (1980) Petrology and geochemistry of composite ultramafic xenoliths in alkalic basalts and implications for magmatic processes within the mantle. American Journal of Science, 280, 389-426.

Jennings, E.S., and Holland, T.J.B. (2015) A Simple Thermodynamic Model for Melting of Peridotite in the System NCFMASOCr. Journal of Petrology, 56, 869-892.

Kang, P., Lamb, W.M., and Drury, M. (2017) Using mineral equilibria to estimate H_2O activities in peridotites from the Western Gneiss Region of Norway. American Mineralogist, 102, 1021-1036.

Karato, S.-i., Paterson, M.S., and FitzGerald, J.D. (1986) Rheology of synthetic olivine aggregates: Influence of grain-size and water. Journal of Geophysical Research, 91, 8151-8176.

King, P.L., Hervig, R.L., Holloway, J.R., Vennemann, T.W., and Righter, K. (1999) Oxy-substitution and dehydrogenation in mantle-derived amphibole megacrysts. Geochimica et Cosmochimica Acta, 63, 3635-3651.

Köhler, T., and Brey, G.P. (1990) Calcium exchange between olivine and clinopyroxene calibrated as a geothermobarometer for natural peridotites from 2 to 60 kb with applications. Geochimica et Cosmochimica Acta, 54, 2375-2388.

Kohlstedt, D.L., and Mackwell, S.J. (1998) Diffusion of hydrogen and intrinsic point defects in olivine. Zeitschrift für physikalische Chemie, 207, 147-162.

Kohlstedt, D.L., Evans, B., and Mackwell, S.J. (1995) Strength of the lithosphere: Constraints imposed by laboratory experiments. Journal of Geophysical Research, 100, 17587-17602.

Kohlstedt, D.L., Keppler, H., and Rubie, D.C. (1996) Solubility of water in the alpha, beta and gamma phases of $(Mg,Fe)_2SiO_4$. Contributions to Mineralogy and Petrology, 123, 345-357.

Lamb, W.M., and Valley, J.W. (1988) Granulite Facies Amphibole and Biotite Equilibria, and Calculated Peak-Metamorphic Water Activities. Contributions to Mineralogy and Petrology, 100, 349-360.

Lamb, W.M., and Popp, R.K. (2009) Amphibole equilibria in mantle rocks: Determining values of mantle aH_2O and implications for mantle H_2O contents. American Mineralogist, 94, 41-52.

Lamb, W.M., Guillemette, R., Popp, R.K., Fritz, S.J., and Chmiel, G.J. (2012) Determination of Fe^{3+}/Fe using the electron microprobe: A calibration for amphiboles. American Mineralogist, 97, 951-961.

Li, Z.X.A., Lee, C.T.A., Peslier, A.H., Lenardic, A., and Mackwell, S.J. (2008) Water contents in mantle xenoliths from the Colorado Plateau and vicinity: Implications for the mantle rheology and hydration-induced thinning of continental lithosphere. Journal of Geophysical Research-Solid Earth, 113.

Luffi, P., Saleeby, J.B., Lee, C.-T.A., and Ducea, M.N. (2009) Lithospheric mantle duplex beneath the central Mojave Desert revealed by xenoliths from Dish Hill, California. Journal of Geophysical Research, 114, B03202.

Mandler, B., and Grove, T.L. (2016) Controls on the stability and composition of amphibole in the Earth's mantle. Contributions to Mineralogy and Petrology, 171.

Marshall, E.W., Lassiter, J.C., and Barnes, J.D. (2018) On the (mis)behavior of water in the mantle: Controls on nominally anhydrous mineral water content in mantle peridotites. Earth and Planetary Science Letters, 499, 219-229.

Matjuschkin, V., Brey, G., Höfer, H., and Woodland, A. (2014) The influence of Fe^{3+} on garnet–orthopyroxene and garnet–olivine geothermometers. Contributions to Mineralogy and Petrology, 167, 1-10.

McGuire, A.V., Dyar, M.D., and Nielson, J.E. (1991) Metasomatic oxidation of upper mantle periodotite. Contributions to Mineralogy and Petrology, 109, 252-264.

Mei, S., and Kohlstedt, D.L. (2000a) Influence of water on plastic deformation of olivine aggregates: 1. Diffusion creep regime. Journal of Geophysical Research, 105, 21457-21469.

-. (2000b) Influence of water on plastic deformation of olivine aggregates: 2. Dislocation creep regime. Journal of Geophysical Research, 105, 21471-21481.

Mierdel, K., and Keppler, H. (2004) The temperature dependence of water solubility in enstatite. Contributions to Mineralogy and Petrology, 148, 305-311.

Miller, W.G.R., Holland, T.J.B., and Gibson, S.A. (2016) Garnet and Spinel Oxybarometers: New Internally Consistent Multi-equilibria Models with Applications to the Oxidation State of the Lithospheric Mantle. Journal of Petrology, 57, 1199-1222.

Mosenfelder, J.L., Deligne, N.I., Asimow, P.D., and Rossman, G.R. (2006) Hydrogen incorporation in olivine from 2–12 GPa. American Mineralogist, 91, 285-294.

Nickel, K., and Green, D. (1985) Empirical geothermobarometry for garnet peridotites and implications for the nature of the lithosphere, kimberlites and diamonds. Earth and Planetary Science Letters, 73, 158-170.

Niida, K., and Green, D. (1999) Stability and chemical composition of pargasitic amphibole in MORB pyrolite under upper mantle conditions. Contributions to Mineralogy and Petrology, 135, 18-40.

Nimis, P., and Taylor, W.R. (2000) Single clinopyroxene thermobarometry for garnet peridotites. Part I. Calibration and testing of a Cr-in-Cpx barometer and an enstatite-in-Cpx thermometer. Contributions to Mineralogy and Petrology, 139, 541-554.

Nimis, P., and Grütter, H. (2010) Internally consistent geothermometers for garnet peridotites and pyroxenites. Contributions to Mineralogy and Petrology, 159, 411-427.

O'Neill, H.S.C. (1981) The transition between spinel lherzolite and garnet lherzolite, and its use as a geobarometer. Contributions to Mineralogy and Petrology, 77, 185-194.

O'Reilly, S.Y., and Griffin, W.L. (2013) Mantle Metasomatism. In Harlov, D.E., and Austrheim, H., Eds. Metasomatism and the Chemical Transformation of Rock, 471-533. Springer, Berlin.

O'Reilly, S.Y., Chen, D., Griffin, W., and Ryan, C. (1997) Minor elements in olivine from spinel lherzolite xenoliths: implications for thermobarometry. Mineralogical Magazine, 61, 257-270.

O'Reilly, S.Y., and Griffin, W.L. (1985) A Xenolith-Derived Geotherm for Southeastern Australia and Its Geophysical Implications. Tectonophysics, 111, 41-63.

Perkins, D., and Anthony, E. (2011) The evolution of spinel lherzolite xenoliths and the nature of the mantle at Kilbourne Hole, New Mexico. Contributions to Mineralogy and Petrology, 162, 1139-1157.

Peslier, A.H. (2010) A review of water contents of nominally anhydrous natural minerals in the mantles of Earth, Mars and the Moon. Journal of Volcanology and Geothermal Research, 197, 239-258.

Peslier, A.H., and Luhr, J.F. (2006) Hydrogen loss from olivines in mantle xenoliths from Simcoe (USA) and Mexico: Mafic alkalic magma ascent rates and water budget of the sub-continental lithosphere. Earth and Planetary Science Letters, 242, 302-319.

Peslier, A.H., Luhr, J.F., and Post, J. (2002) Low water contents in pyroxenes from spinel-peridotites of the oxidized, sub-arc mantle wedge. Earth and Planetary Science Letters, 201, 69-86.

Peslier, A.H., Schönbächler, M., Busemann, H., and Karato, S.I. (2017) Water in the Earth's Interior: Distribution and Origin. Space Science Reviews, 212, 743-810.

Pollack, H., and Sass, J. (1988) Thermal regime of the lithosphere. Handbook of Terrestrial Heat-Flow Density Determination, 301-308.

Popp, R.K., and Phillips, M.W. (1995) An experimental study of phase equilibria and Fe oxy-component in kaersutitic. American Mineralogist, 80, 534-548.

Popp, R.K., Virgo, D., and Phillips, M.W. (1995a) H deficiency in kaersutitic amphiboles: Experimental verification. American Mineralogist, 80, 1347-1350.

Popp, R.K., Hibbert, H.A., and Lamb, W.M. (2006) Oxy-amphibole equilibria in Ti-bearing calcic amphiboles: Experimental investigation and petrologic implications for mantle-derived amphiboles. American Mineralogist, 91, 54-66.

Popp, R.K., Virgo, D., Yoder, H.S., Hoering, T.C., and Phillips, M.W. (1995b) An Experimental-Study of Phase-Equilibria and Fe Oxy-Component in Kaersutitic

Amphibole - Implications for the fH_2 and aH_2O in the Upper-Mantle. American Mineralogist, 80, 534-548.

Powell, R., Holland, T., and Worley, B. (1998) Calculating phase diagrams involving solid solutions via non‐linear equations, with examples using THERMOCALC. Journal of Metamorphic Geology, 16, 577-588.

Quinn, R.J., Valley, J.W., Page, F.Z., and Fournelle, J.H. (2016) Accurate determination of ferric iron in garnets. American Mineralogist, 101, 1704-1707.

Riter, J.C.A. (1999) Geochemical and tectonic evolution of the Colorado Plateau mantle lithosphere: Evidence from Grand Canyon mantle xenoliths. Ph.D. Dissertation, The University of Texas at Austin, 356 pages.

Sack, R., and Ghiorso, M. (1994a) Thermodynamics of multicomponent pyroxenes: II. Phase relations in the quadrilateral. Contributions to Mineralogy and Petrology, 116, 287-300.

-. (1994b) Thermodynamics of multicomponent pyroxenes: I. Formulation of a general model. Contributions to Mineralogy and Petrology, 116, 277-286.

Sack, R.O., and Ghiorso, M.S. (1989) Importance of considerations of mixing properties in establishing an internally consistent thermodynamic database: thermochemistry of minerals in the system Mg_2SiO_4-Fe_2SiO_4-SiO_2. Contributions to Mineralogy and Petrology, 102, 41-68.

Sack, R.O., and Ghiorso, M.S. (1991) An internally consistent model for the thermodynamic properties of Fe−Mg-titanomagnetite-aluminate spinels. Contributions to Mineralogy and Petrology, 106, 474-505.

Satsukawa, T., Michibayashi, K., Anthony, E.Y., Stern, R.J., Gao, S.S., and Liu, K.H. (2011) Seismic anisotropy of the uppermost mantle beneath the Rio Grande rift: Evidence from Kilbourne Hole peridotite xenoliths, New Mexico. Earth and Planetary Science Letters, 311, 172-181.

Schumacher, J.C. (1991) Empirical ferric iron corrections: necessity, assumptions, and effects on selected geothermobarometers. Mineralogical Magazine, 55, 3-18.

Skogby, H. (2006) Water in natural mantle minerals I: pyroxenes. In Keppler, H., and Smyth, J.R., Eds. Water in Nominally Anhydrous Minerals, 62, 155-167. Mineralogical Society of America.

Smith, D. (1999) Temperatures and pressures of mineral equilibration in peridotite xenoliths: review, discussion, and implications. Mantle petrology: field observations and high pressure experimentation: a tribute to Francis R.(Joe) Boyd. Geochemical Society Special Publication, 6, 3-12.

Smyth, J., Bell, D., and Rossman, G. (1991) Incorporation of hydroxyl in upper-mantle clinopyroxenes. Nature, 351, 732-735.

Smyth, J.R., Mierdel, K., Keppler, H., Langenhorst, F., Dubrovinsky, L., and Nestola, F. (2007) Crystal chemistry of hydration in aluminous orthopyroxene. American Mineralogist, 92, 973-976.

Spear, F.S. (1995) Metamorphic phase equilibria and pressure-temperature-time paths. Mineralogical Society of America Washington.

Stalder, R. (2004) Influence of Fe, Cr and Al on hydrogen incorporation in orthopyroxene. European Journal of Mineralogy, 16, 703-711.

Stalder, R., Kronz, A., and Simon, K. (2008) Hydrogen incorporation in enstatite in the system MgO-SiO_2-H_2O-NaCl. Contributions to Mineralogy and Petrology, 156, 653-659.

Su, B., Zhang, H., Asamoah, S.P., Qin, K., Tang, Y., Ying, J., and Xiao, Y. (2010) Garnet-spinel transition in the upper mantle: Review and interpretation. Journal of Earth Science, 21, 635-640.

Taylor, W. (1998) An experimental test of some geothermometer and geobarometer formulations for upper mantle peridotites with application to the thermobarometry of fertile lherzorite and garnet websterite. Neues Jahrbuch feur Mineralogie Abhandlungen, 172, 381-408.

Wang, D., Mookherjee, M., Xu, Y., and Karato, S.-i. (2006) The effect of water on the electrical conductivity of olivine. Nature, 443, 977-980.

Warren, J.M., and Hauri, E.H. (2014) Pyroxenes as tracers of mantle water variations. Journal of Geophysical Research: Solid Earth, 119, 1851-1881.

Wells, P.R. (1977) Pyroxene thermometry in simple and complex systems. Contributions to mineralogy and Petrology, 62, 129-139.

White, R., Powell, R., and Clarke, G. (2002) The interpretation of reaction textures in Fe‐rich metapelitic granulites of the Musgrave Block, central Australia: constraints from mineral equilibria calculations in the system K_2O–FeO–MgO–Al_2O_3–SiO_2–H_2O–TiO_2–Fe_2O_3. Journal of metamorphic Geology, 20, 41-55.

Wilshire, H., Calk, L., and Schwarzman, E.C. (1971) Kaersutite—a product of reaction between pargasite and basanite at Dish Hill, California. Earth and Planetary Science Letters, 10, 281-284.

Wilshire, H., Pike, J.N., Meyer, C., and Schwarzman, E. (1980) Amphibole-rich veins in lherzolite xenoliths, Dish Hill and Deadman Lake, California. American Journal of Science, 280, 576-593.

Wilshire, H.G., and Trask, N.J. (1971) Structural and textural relationships of amphibole and phlogopite in peridotite inclusions, Dish Hill, California. American Mineralogist, 56, 240-255.

Wood, B.J. (1990) An experimental test of the spinel peridotite oxygen barometer. Journal of Geophysical Research, 95, 15845-15851.

Wood, B.J., and Virgo, D. (1989a) Upper mantle oxidation state: Ferric iron contents of lherzolite spinels by ^{57}Fe Mossbauer spectroscopy and resultant oxygen fugacities. Geochimica et Cosmochimica Acta, 53, 1277-1291.

Wood, B.J., and Virgo, D. (1989b) Upper mantle oxidation state: Ferric iron contents of Iherzolite spinels by 57 Fe Mössbauer spectroscopy and resultant oxygen fugacities. Geochimica et Cosmochimica Acta, 53, 1277-1291.

Wood, B.J., Bryndzia, L.T., and Johnson, K.E. (1990) Mantle oxidation state and its relationship to tectonic environment and fluid speciation. Science, 248, 337-345.

Woodland, A.B., and Koch, M. (2003) Variation in oxygen fugacity with depth in the upper mantle beneath the Kaapvaal craton, Southern Africa. Earth and Planetary Science Letters, 214, 295-310.

Woodland, A.B., Kornprobst, J., and Wood, B.J. (1992) Oxygen thermobarometry of orogenic lherzolite massifs. Journal of Petrology, 33, 203-230.

Wyllie, P.J. (1979) Magmas and volatile components. American Mineralogist, 64, 469-500.

Xu, X., OReilly, S.Y., Zhou, X., and Griffin, W.L. (1996) A xenolith-derived geotherm and the crust-mantle boundary at Qilin, southeastern China. Lithos, 38, 41-62.

Yoshino, T., Matsuzaki, T., Shatskiy, A., and Katsura, T. (2009) The effect of water on the electrical conductivity of olivine aggregates and its implications for the electrical structure of the upper mantle. Earth and Planetary Science Letters, 288, 291-300.

Zhao, C., and Yoshino, T. (2016) Electrical conductivity of mantle clinopyroxene as a function of water content and its implication on electrical structure of uppermost mantle. Earth and Planetary Science Letters, 447, 1-9.

Zhao, Y.-H., Ginsberg, S.B., and Kohlstedt, D.L. (2004) Solubility of hydrogen in olivine: dependence on temperature and iron content. Contributions to Mineralogy and Petrology, 147, 155-161.

This is a preprint, the final version is subject to change, of the American Mineralogist (MSA)
Cite as Authors (Year) Title. American Mineralogist, in press.
DOI: https://doi.org/10.2138/am-2019-6602

Table 1: Selected Olivine Analyses (wt. %).

Sample:	X174	X192	X229	X286	X297	X299
SiO_2	38.39	39.45	39.97	39.44	39.48	39.71
FeO	21.45	15.92	15.62	16.94	16.06	15.38
MnO	0.15	0.20	0.20	0.20	0.20	0.20
MgO	40.17	44.50	44.78	43.19	44.04	44.52
NiO	0.10	0.16	0.13	0.16	0.15	0.14
SUM	100.25	100.22	100.70	99.93	99.92	99.95
Mg #	0.77	0.83	0.84	0.82	0.83	0.83

Sample:	X319	Ba-1-72	Ba-2-1-1	EP-3-84	TF6
SiO_2	39.40	40.45	40.81	40.42	40.41
FeO	15.17	11.52	9.33	11.86	9.43
MnO	0.19	0.18	0.14	0.17	0.13
MgO	45.02	47.81	49.21	47.11	49.32
NiO	0.16	0.33	0.38	0.31	0.40
SUM	99.94	100.29	99.88	99.87	99.68
Mg#	0.84	0.88	0.90	0.88	0.90

Normalized mineral formulae available in the electronic supplement

This is a preprint, the final version is subject to change, of the American Mineralogist (MSA)
Cite as Authors (Year) Title. American Mineralogist, in press.
DOI: https://doi.org/10.2138/am-2019-6602

Table 2: Selected Amphibole Analyses (wt. %).

Sample:	X174	X192	X229	X286	X297	X299	X319	Ba-1-72	Ba2-1-1	EP-3-84	TF6
Textures	d,r	p	p	p	p	d,r	p	d,r	d,r	d,r	d,r
SiO_2	40.80	41.42	41.14	41.78	41.48	42.06	41.20	42.83	43.16	41.65	43.38
TiO_2	3.36	3.46	2.63	3.28	2.64	2.08	2.79	1.42	1.77	3.38	0.28
Al_2O_3	15.64	15.63	15.82	14.97	15.31	15.65	15.41	15.56	15.60	15.66	15.29
Cr_2O_3	bdl	0.36	bdl	0.25	0.33	0.32	0.28	1.08	1.10	bdl	1.32
FeO	8.37	6.36	6.94	7.58	6.63	6.70	6.16	5.28	4.34	5.53	4.07
MgO	15.01	15.93	16.10	15.22	16.30	16.42	16.59	17.33	17.92	16.63	18.59
CaO	11.14	11.03	11.69	11.09	11.53	11.47	11.68	10.71	10.56	11.42	11.41
Na_2O	3.31	2.99	2.41	2.71	1.96	2.67	2.71	3.34	3.77	3.30	3.16
K_2O	0.70	1.40	1.08	1.20	1.18	0.56	1.18	0.73	0.05	0.45	0.49
F	bdl	bdl	bdl	bdl	bdl	bdl	bdl	0.21	bdl	0.33	bdl
Cl	bdl	bdl	bdl	bdl	bdl	bdl	bdl	bdl	bdl	bdl	bdl
H_2O	1.88	1.79	1.77	1.69	1.77	1.85	1.89	1.84	1.91	1.55	2.08
Sum	100.21	100.37	99.58	99.77	99.13	99.78	99.89	100.33	100.18	99.90	100.07
O=F	0.00	0.00	0.00	0.00	0.00	0.00	0.00	0.09	0.00	0.14	0.00
Sum	100.21	100.37	99.58	99.77	99.13	99.78	99.89	100.24	100.18	99.76	100.07
Fe^{3+}/Fe_{Total}	0.23	0.42	0.25	0.36	0.35	0.42	0.29	0.25	nm	0.43	nm

Textures: d, disseminated, r, rimming spinel, p, poikilitic.
bdl, concentration below detection limit

This is a preprint, the final version is subject to change, of the American Mineralogist (MSA)
Cite as Authors (Year) Title. American Mineralogist, in press.
DOI: https://doi.org/10.2138/am-2019-6602

Table 3: Selected Clinopyroxene Analyses (wt. %).

Sample:	X174	X192	X229	X286	X297		X299		X319	Ba-1-72		Ba2-1-1	EP-3-84		TF6
	Avg	Avg	Avg	Avg	Core	Rim	Core	Rim	Avg	Core	Rim	Avg	Core	Rim	Avg
SiO_2	49.92	49.29	49.27	51.57	49.41	50.22	49.54	50.18	49.12	50.97	51.69	51.33	48.67	48.91	52.14
TiO_2	1.09	1.15	1.04	0.74	0.94	0.90	0.90	0.80	1.13	0.53	0.33	0.43	1.28	1.25	0.07
Al_2O_3	6.08	7.50	7.66	5.11	7.15	5.71	7.42	6.60	7.63	7.28	6.46	6.87	8.56	7.84	4.32
Cr_2O_3	bdl	0.19	bdl	0.14	0.31	0.25	0.23	0.21	0.18	0.87	0.69	0.81	bdl	bdl	0.51
FeO	6.12	4.57	3.44	5.64	5.15	4.93	4.99	4.78	4.94	4.16	3.93	3.15	4.30	4.21	2.91
MgO	14.86	15.15	14.63	15.26	14.92	15.62	14.66	15.11	15.45	15.28	15.70	15.62	14.58	14.69	17.16
CaO	20.74	21.31	21.90	20.95	21.67	21.99	21.89	21.97	20.46	20.25	20.14	20.18	20.82	21.20	22.00
Na_2O	0.97	0.78	0.52	0.89	0.52	0.53	0.53	0.44	0.60	1.47	1.44	1.48	1.02	0.96	0.67
Sum	99.80	99.95	98.45	100.30	100.07	100.15	100.14	100.09	99.51	100.82	100.39	99.88	99.23	99.06	99.78
Fe_2O_3	3.37	2.81	0.15	1.63	2.24	2.84	1.72	1.33	1.91	3.07	2.55	2.17	2.62	2.66	2.63
FeO	3.10	2.05	3.30	4.17	3.13	2.38	3.44	3.58	3.23	1.40	1.64	1.20	1.95	1.82	0.55
Sum	100.14	100.23	98.47	100.46	100.30	100.44	100.31	100.23	99.70	101.13	100.65	100.10	99.49	99.33	100.05
Mg#	0.81	0.86	0.88	0.83	0.84	0.85	0.84	0.85	0.85	0.87	0.88	0.90	0.86	0.86	0.91
Fe^{3+}/Fe_{Tot}	0.49	0.55	0.04	0.26	0.39	0.52	0.31	0.25	0.35	0.66	0.58	0.62	0.55	0.57	0.81

bdl, concentration below detection limit;
Normalized mineral formulae available in the electronic supplement

This is a preprint, the final version is subject to change, of the American Mineralogist (MSA)
Cite as Authors (Year) Title. American Mineralogist, in press.
DOI: https://doi.org/10.2138/am-2019-6602

Table 4: Selected Orthopyroxene Analyses (wt. %).

Sample:	X174	X192		X229	X286		X297		X299		X319		Ba-1-72	Ba2-1-1	EP-3-84	TF6
	Avg	Core	Rim	Avg	Core	Rim	Core	Rim	Core	Rim	Core	Rim	Avg	Avg	Avg	Avg
SiO_2	52.21	52.74	53.26	51.81	52.90	53.12	51.74	52.34	51.66	52.53	52.10	52.42	53.30	54.87	54.25	54.69
TiO_2	0.32	0.36	0.32	0.26	0.34	0.34	0.34	0.30	0.29	0.22	0.37	0.35	0.09	0.11	0.20	0.01
Al_2O_3	5.43	5.41	4.94	5.72	4.88	4.47	6.39	5.48	6.28	5.78	6.31	5.89	4.69	4.79	4.86	4.26
Cr_2O_3	bdl	0.05	bdl	bdl	0.12	0.12	0.17	0.19	0.15	0.15	0.14	0.13	0.34	0.38	0.18	0.43
FeO	12.63	10.65	11.00	10.62	10.61	10.54	10.45	10.64	10.25	10.18	9.69	9.66	7.58	6.18	7.65	6.26
MgO	27.98	28.99	29.15	29.52	30.14	30.39	29.80	29.74	29.94	30.32	29.65	29.96	32.65	32.48	31.65	32.85
CaO	0.84	1.10	0.81	0.74	0.87	0.84	0.76	0.77	0.76	0.74	0.80	0.76	0.92	0.81	0.71	0.72
Na_2O	0.06	0.11	0.10	0.03	bdl	0.05	0.05	0.04	0.05	bdl	0.04	0.03	0.11	0.10	0.06	0.04
Sum	99.48	99.41	99.57	98.70	99.86	99.87	99.70	99.50	99.38	99.92	99.10	99.20	99.68	99.72	99.56	99.26
Fe_2O_3	1.26	0.96	0.50	2.39	2.10	2.44	2.90	2.19	3.11	2.41	1.25	1.32	4.10	0.00	0.23	0.58
FeO	11.49	9.79	10.55	8.48	8.72	8.34	7.85	8.67	7.46	8.01	8.57	8.48	3.90	6.18	7.44	5.74
Sum	99.60	99.51	99.62	98.94	100.07	100.12	99.99	99.72	99.70	100.16	99.23	99.33	100.09	99.72	99.58	99.32
Mg#	0.80	0.83	0.83	0.83	0.84	0.84	0.84	0.83	0.84	0.84	0.85	0.85	0.88	0.90	0.88	0.90
Fe^{3+}/Fe_{Total}	0.09	0.08	0.04	0.20	0.18	0.21	0.25	0.19	0.27	0.21	0.12	0.12	0.49	0.00	0.03	0.08

bdl, concentration below the detection limit;
Normalized mineral formulae available in the electronic supplement

Table 5: Selected Spinel Analyses (wt. %).

Sample:	X174	X192	X229	X286		X297		X299	X319	Ba-1-72	Ba2-1-1	EP-3-84	TF6
	Avg	Avg	Avg	Core	Rim	Core	Rim	Avg	Avg	Avg	Avg	Avg	Avg
SiO_2	0.07	0.06	0.06	bdl	0.06	0.05	bdl	bdl	0.06	0.07	0.08	0.05	0.06
TiO_2	0.58	0.48	0.36	0.33	0.37	0.57	0.48	0.36	0.45	0.08	0.08	0.16	bdl
Al_2O_3	59.49	58.36	60.91	55.68	55.11	54.63	55.12	57.93	58.87	53.00	55.80	64.22	49.76
Cr_2O_3	0.15	4.57	0.89	6.89	6.81	6.13	6.01	3.23	3.48	11.62	10.61	bdl	16.05
FeO	22.41	17.72	18.68	18.53	19.52	21.97	20.96	19.36	17.71	15.57	11.44	14.10	13.47
MnO	0.08	0.25	0.13	0.21	0.21	0.21	0.18	0.14	0.22	0.20	0.36	0.11	0.57
MgO	16.65	17.99	18.83	17.74	17.74	17.12	17.37	18.08	18.60	19.39	20.82	20.65	19.52
NiO	0.16	0.20	0.17	0.23	0.23	0.24	0.28	0.21	0.22	0.36	0.40	0.25	0.37
ZnO	0.23	0.14	bdl	0.18	0.26	bdl	bdl	bdl	0.14	0.12	bdl	bdl	bdl
Sum	99.84	99.76	100.02	99.79	100.49	100.90	100.61	99.30	99.75	100.41	99.61	99.58	99.80
Fe_2O_3	5.84	3.54	6.47	5.67	6.69	7.71	8.21	6.82	4.60	6.11	2.94	3.56	4.23
FeO	17.16	14.54	12.85	13.43	13.51	15.03	14.10	13.22	13.57	10.08	8.79	10.90	9.67
Sum	100.58	100.23	100.67	100.36	100.90	101.67	101.51	99.99	100.34	101.02	99.90	99.94	100.37
Mg#	0.65	0.70	0.72	0.70	0.70	0.67	0.67	0.71	0.72	0.77	0.82	0.78	0.79
Cr#	0.002	0.050	0.010	0.077	0.077	0.070	0.068	0.036	0.038	0.128	0.113	0.000	0.178
Fe^{3+}/Fe_{Tot}	0.23	0.18	0.31	0.28	0.31	0.33	0.34	0.32	0.23	0.35	0.23	0.23	0.28

bdl, concentration below the detection limit;
Normalized mineral formulae available in the electronic supplement

This is a preprint, the final version is subject to change, of the American Mineralogist (MSA)
Cite as Authors (Year) Title. American Mineralogist, in press.
DOI: https://doi.org/10.2138/am-2019-6602

Table 6: Estimated temperatures (˚C) at pressures of 1.1 and 1.5 GPa

Sample:	T98[a]		NT[b]		BKNG[c]	
	1.1	1.5	1.1	1.5	1.1	1.5
X174	**930**	940	950	960	990	1010
X192	**910**	930	940	960	970	1000
X229	**880**	900	900	900	950	970
X286	**950**	960	970	970	980	1000
X297	**920**	930	940	950	960	980
X299	**930**	940	950	950	950	970
X319	**920**	940	950	960	950	980
Ba-1-72	960	**980**	990	1000	1000	1030
Ba2-1-1	950	**960**	970	980	970	990
EP-3-84	**870**	880	900	910	930	950
TF6	**940**	960	970	980	940	960

(a) Taylor (1998) 2-Px (b) Nimis and Taylor (2000) - En-in-cpx
(c) Nimis and Grutter (2010) - modified B&K Ca-in-opx
Temperatures in bold were used in the construction of Figures.

This is a preprint, the final version is subject to change, of the American Mineralogist (MSA)
Cite as Authors (Year) Title. American Mineralogist, in press.
DOI: https://doi.org/10.2138/am-2019-6602

Table 7: Values of aH_2O estimated using Methods A and B at 1.1 and 1.5 GPa.

	Method A		Method B	
	1.1	1.5	1.1	1.5
X174	0.03	0.04	**0.07**	0.08
X192	0.03	0.04	**0.06**	0.07
X229	0.05	0.08	**0.08**	0.11
X286	0.03	0.04	**0.04**	0.05
X297	0.03	0.04	**0.04**	0.05
X299	0.05	0.07	**0.12**	0.14
X319	0.06	0.09	**0.12**	0.16
Ba-1-72	0.03	0.04	0.09	**0.12**
Ba2-1-1	0.03	0.04	0.12	**0.15**
EP-3-84	0.02	0.03	**0.05**	0.06
TF6	0.09	0.12	**0.19**	0.26

This is a preprint, the final version is subject to change, of the American Mineralogist (MSA)
Cite as Authors (Year) Title. American Mineralogist, in press.
DOI: https://doi.org/10.2138/am-2019-6602

Table 8: Values of fO_2, fH_2 and aH_2O (from a combination of fO_2 and fH_2) estimated at two pressures.

Sample:	Δlog fO_2 (FMQ)	fH_2 (bars)	aH_2O	Δlog fO_2 (FMQ)	fH_2 (bars)	aH_2O	Δlog fO_2 (FMQ)	fH_2 (bars)	aH_2O	Δlog fO_2 (FMQ)	fH_2 (bars)	aH_2O
	Miller at 1.1 GPa			Miller at 1.5 GPa			Wood at 1.1 GPa			Wood at 1.5 GPa		
X174	0.12	34	0.12	-0.12	69	0.19	**-0.30**	34	**0.07**	-0.44	69	0.12
X192	-0.19	3	0.01	-0.45	8	0.01	**0.00**	3	**0.01**	-0.16	8	0.02
X229	0.88	14	0.13	0.62	27	0.20	**0.54**	14	**0.09**	0.38	32	0.11
X286	0.31	6	0.03	0.08	13	0.04	**-0.20**	6	**0.02**	-0.33	13	0.03
X297	0.80	7	0.06	0.58	15	0.09	**0.53**	7	**0.04**	0.39	15	0.07
X299	0.82	3	0.02	0.60	6	0.04	**0.48**	3	**0.01**	0.34	6	0.03
X319	0.40	18	0.11	0.17	40	0.15	**0.04**	18	**0.06**	-0.12	40	0.11
Ba-1-72	0.84	44	0.34	0.63	91	0.57	-0.66	44	0.06	**-0.81**	91	**0.11**
Ba2-1-1	0.22	nm	nm	0.01	nm	nm	0.41	nm	nm	**0.27**	nm	nm
EP-3-84	0.84	3	0.03	0.58	6	0.04	**0.67**	**3**	**0.02**	0.52	6	0.04
TF6	0.69	nm	nm	0.46	nm	nm	**0.61**	nm	nm	0.47	nm	nm

nm - Values of fH_2 not estimated for samples Ba2-1-1 and TF6 (see text for explanation).
Values in bold were used for the construction of Figures.

This is a preprint, the final version is subject to change, of the American Mineralogist (MSA)
Cite as Authors (Year) Title. American Mineralogist, in press.
DOI: https://doi.org/10.2138/am-2019-6602

Table 9: Predicted H_2O contents of olivine.

Sample:	M[1]	Z[2]	G[3]	M[1]	Z[2]	G[3]
	1.1 GPa			1.5 GPa		
X174	8	19	9	13	33	13
X192	6	8	8	12	15	11
X229	8	9	9	17	20	15
X286	5	7	7	9	14	10
X297	4	6	6	8	11	10
X299	13	16	13	23	30	19
X319	13	15	12	27	33	20
Ba-1-72	10	9	11	21	20	18
Ba2-1-1	14	9	13	26	19	19
EP-3-84	5	3	7	9	7	10
TF6	29	20	17	45	32	28

(1) Mosenfelder et al. (2006) (2) Zhao et al. (2004)
(3) Gaetani et al. (2014); H_2O contents in ppm(w)

This is a preprint, the final version is subject to change, of the American Mineralogist (MSA)
Cite as Authors (Year) Title. American Mineralogist, in press.
DOI: https://doi.org/10.2138/am-2019-6602

Figure Captions

Figure 1: The Fe^{3+}/Fe_{Total} of opx as estimated by requiring a charge balanced mineral formula (chemical information from EMPA). These results suggest that the precision of this method is sufficient to differentiate values of Fe^{3+}/Fe_{Total} between samples, often to better than 0.1.

Figure 2: Map illustrating the sample locations (denoted by the black-filled stars) for the 11 mantle xenoliths examined in this study. 8 samples are from the Grand Canyon, Arizona. 2 samples are from Dish Hill, California and 1 sample is from Kilbourne Hole, New Mexico.

Figure 3: Photomicrographs illustrating typical mineralogies and textures. Amphibole occurs in varying amounts in these samples and also in three different textural relations: (1) disseminated grains, (2) grains rimming spinel, and (3) poikilitic. (a) Sample X192 contains abundant amphibole (A) and olivine (Ol) with lesser amounts of orthopyroxene (Opx), clinopyroxene (Cpx), and spinel (Sp). (b) Sample X174 is the only garnet-bearing (Gt) sample examined in this study. It is opx-rich with amphibole rimming spinel and occurring as disseminated grains. (c) Sample X229 contains abundant amphibole (poikilitic), cpx and sp. (d) Sample Ba-1-72 is olivine-rich and includes amphibole that occurs rimming spinel and as disseminated individual grains.

Figure 4: Mineral compositions plotted as a function of distance, vertical axes represent locations of grain boundaries. (a) Relative depletion in Al and enrichment in Si is sometimes apparent at grain boundaries as illustrated by this opx grain from sample X299. (b) Similar to the opx in sample X299, cpx from sample EP-3-84 exhibit core to rim variations where the rims are depleted in Al and enriched in both Si and Ca.

Figure 5: Values of fO_2 have been estimated using the oxy-barometer of Wood (1990) and are expressed relative to the FMQ oxygen buffer at temperatures from 880 to 980˚C. The values of $\Delta \log fO_2$ range from 1 log unit below, to 0.7 log units above FMQ.

Figure 6: A comparison of the values of aH_2O estimated using amphibole dehydration equilibria (Method B) and the combination of fO_2 and fH_2 (referred to as the combined approach, see text). Both methods yield values of aH_2O that are less than 0.20, and of these values agree within uncertainty.

Figure 7: Values of aH_2O estimated using amphibole dehydration equilibria and the combination of dehydrogenation and redox equilibria (combined approach). Circles indicate current values of amphibole H-content and the corresponding estimated values of aH_2O. If the amphibole suffered retrograde H-loss then this mineral originally contained more OH and the estimate values of aH_2O would have been greater. However, the change in aH_2O with increased H-content is much greater for the combined approach (curve) than for values of aH_2O estimated using dehydration equilibria (line). This rapid divergence in values of aH_2O supports the argument this amphibole did not experience significant retrograde H-loss from (see text).

Figure 8: Values of $\Delta \log fO_2$ (FMQ) plotted as a function of the Fe^{3+}/Fe_{Total} ratio for mantle amphiboles. The filled symbols represent samples in this study from the SW USA (this study; Lamb & Popp (2009), & McGuire *et al.* (1991). The remaining open squares represent data from Antarctica, which have been recalculated using the same T and fO_2 methods described in this paper (Gentili *et al.* (2015) & Bonadiman *et al.* (2014)). Error bars have been omitted for clarity, the uncertainty in values of fO_2 typically are $< \pm 0.55$ log units except for samples X192 (±0.8), EP-3-84 (±0.9), and Ba-1-72 (±1.5). Uncertainty in values of Fe^{3+}/Fe_{Total} are approximately ± 0.07.

This is a preprint, the final version is subject to change, of the American Mineralogist (MSA)
Cite as Authors (Year) Title. American Mineralogist, in press.
DOI: https://doi.org/10.2138/am-2019-6602

Figure 1

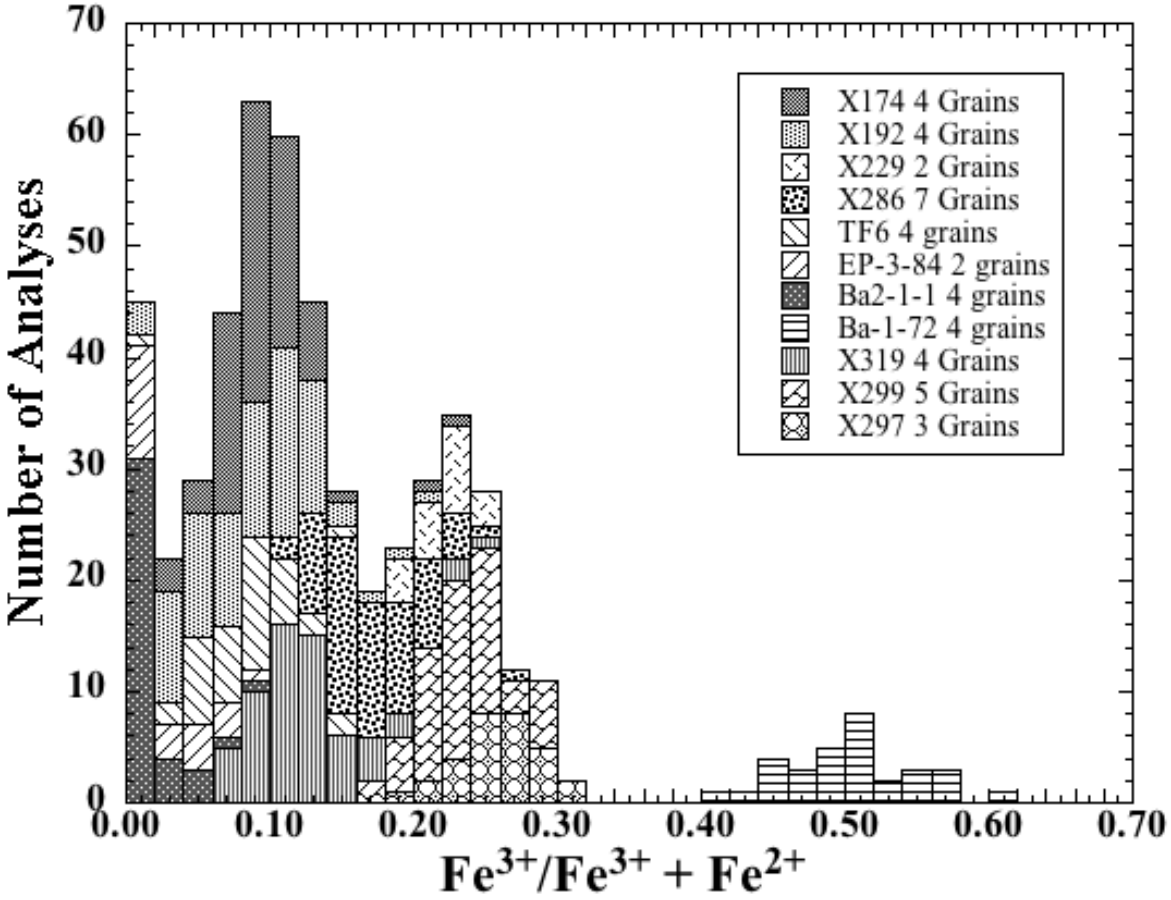

This is a preprint, the final version is subject to change, of the American Mineralogist (MSA)
Cite as Authors (Year) Title. American Mineralogist, in press.
DOI: https://doi.org/10.2138/am-2019-6602

Figure 2

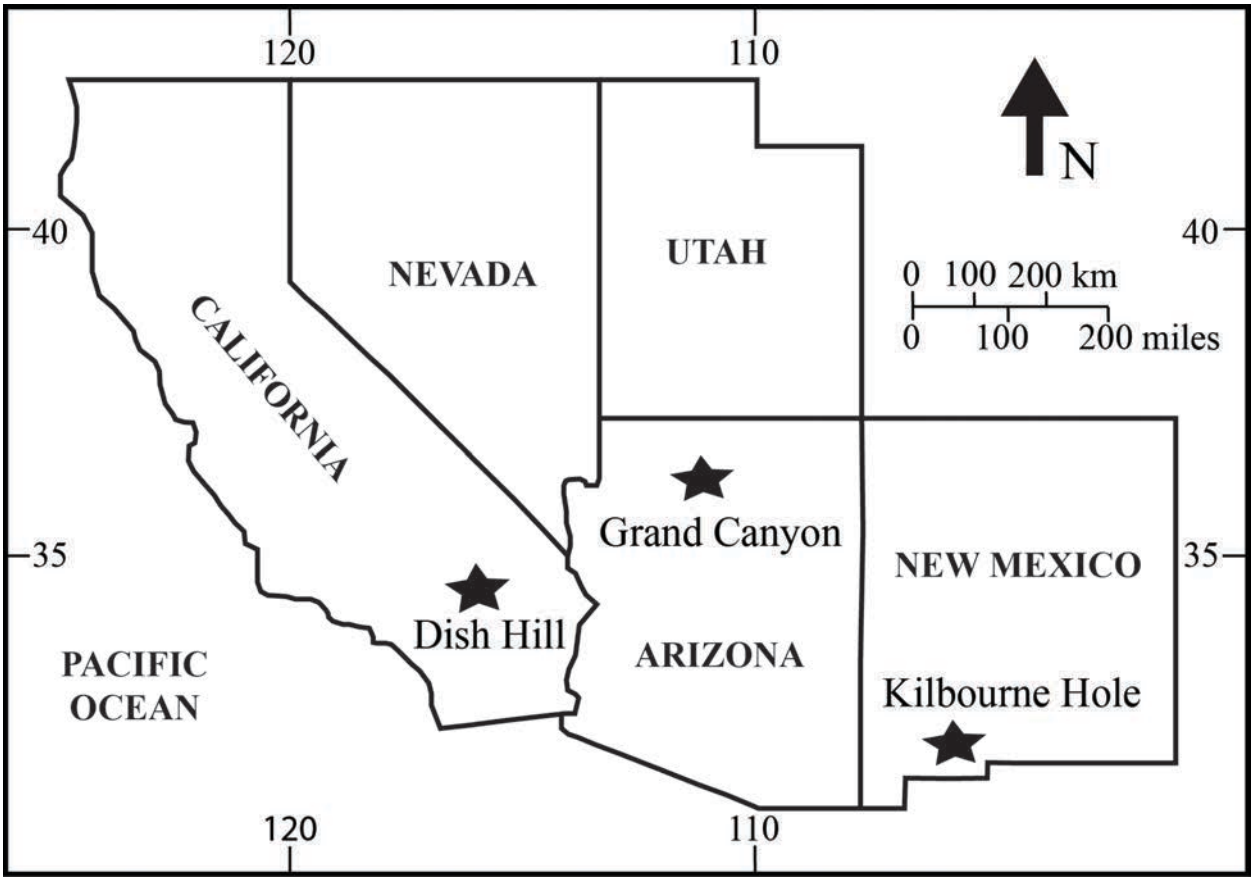

This is a preprint, the final version is subject to change, of the American Mineralogist (MSA)
Cite as Authors (Year) Title. American Mineralogist, in press.
DOI: https://doi.org/10.2138/am-2019-6602

Figure 3

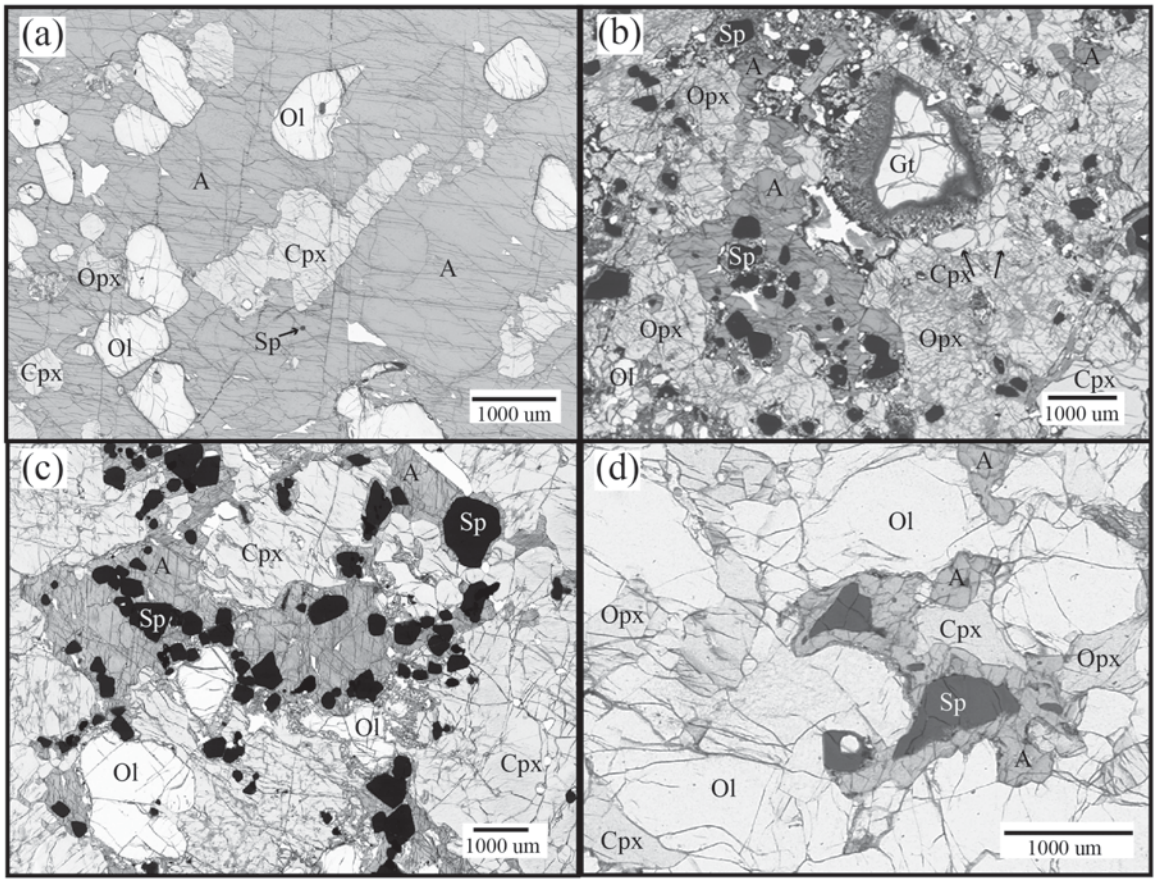

This is a preprint, the final version is subject to change, of the American Mineralogist (MSA)
Cite as Authors (Year) Title. American Mineralogist, in press.
DOI: https://doi.org/10.2138/am-2019-6602

Figure 4

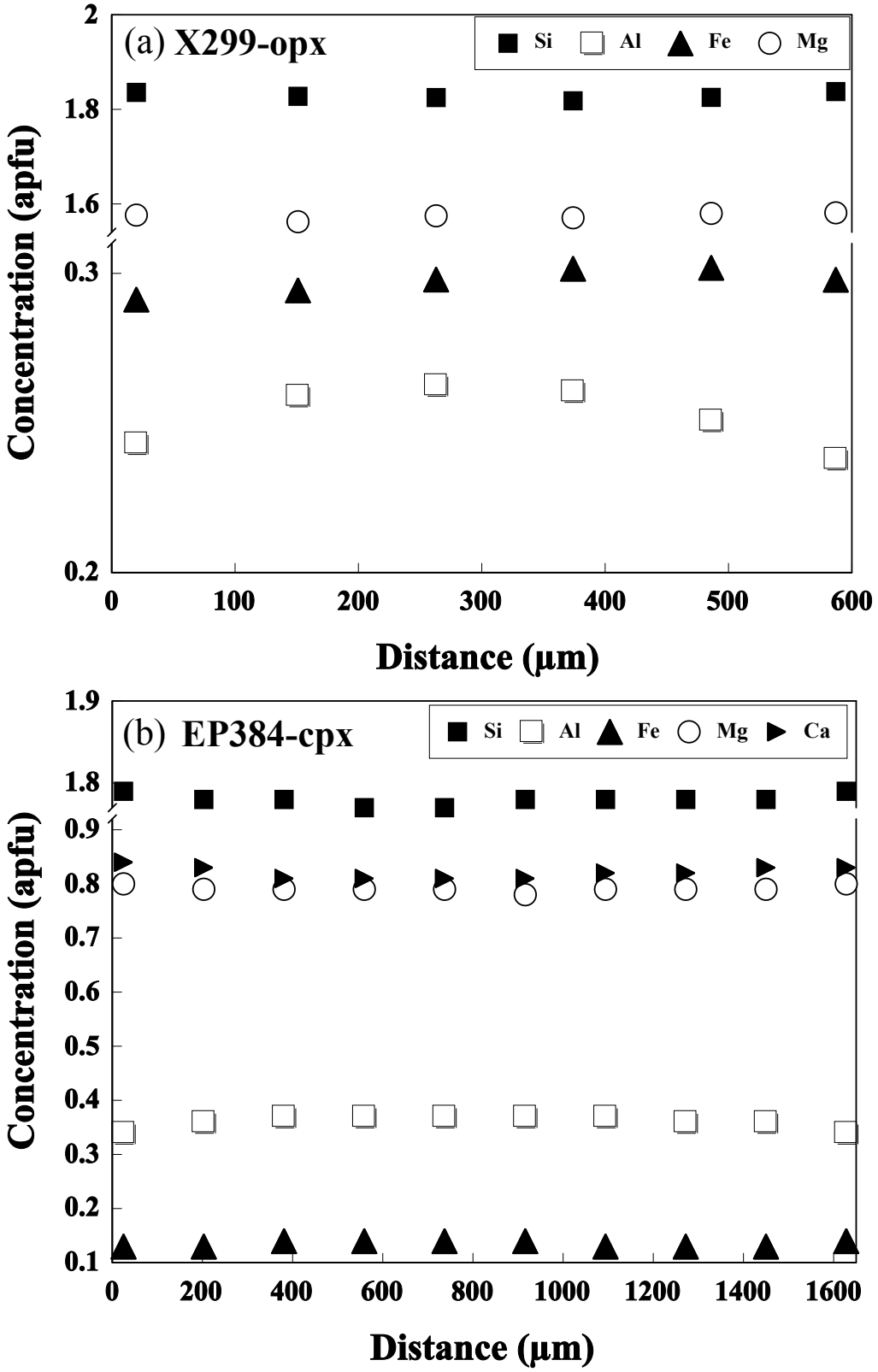

This is a preprint, the final version is subject to change, of the American Mineralogist (MSA)
Cite as Authors (Year) Title. American Mineralogist, in press.
DOI: https://doi.org/10.2138/am-2019-6602

Figure 5

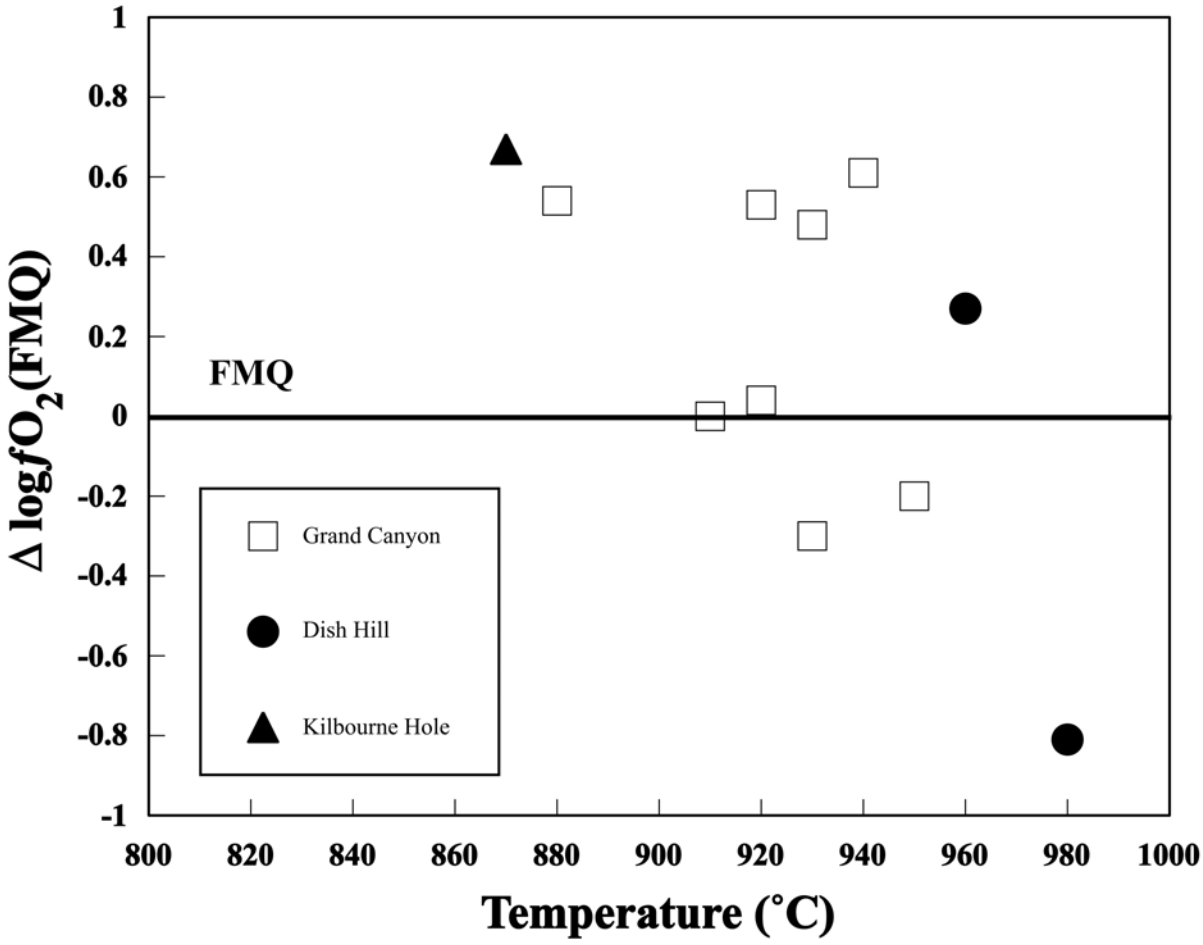

This is a preprint, the final version is subject to change, of the American Mineralogist (MSA)
Cite as Authors (Year) Title. American Mineralogist, in press.
DOI: https://doi.org/10.2138/am-2019-6602

Figure 6

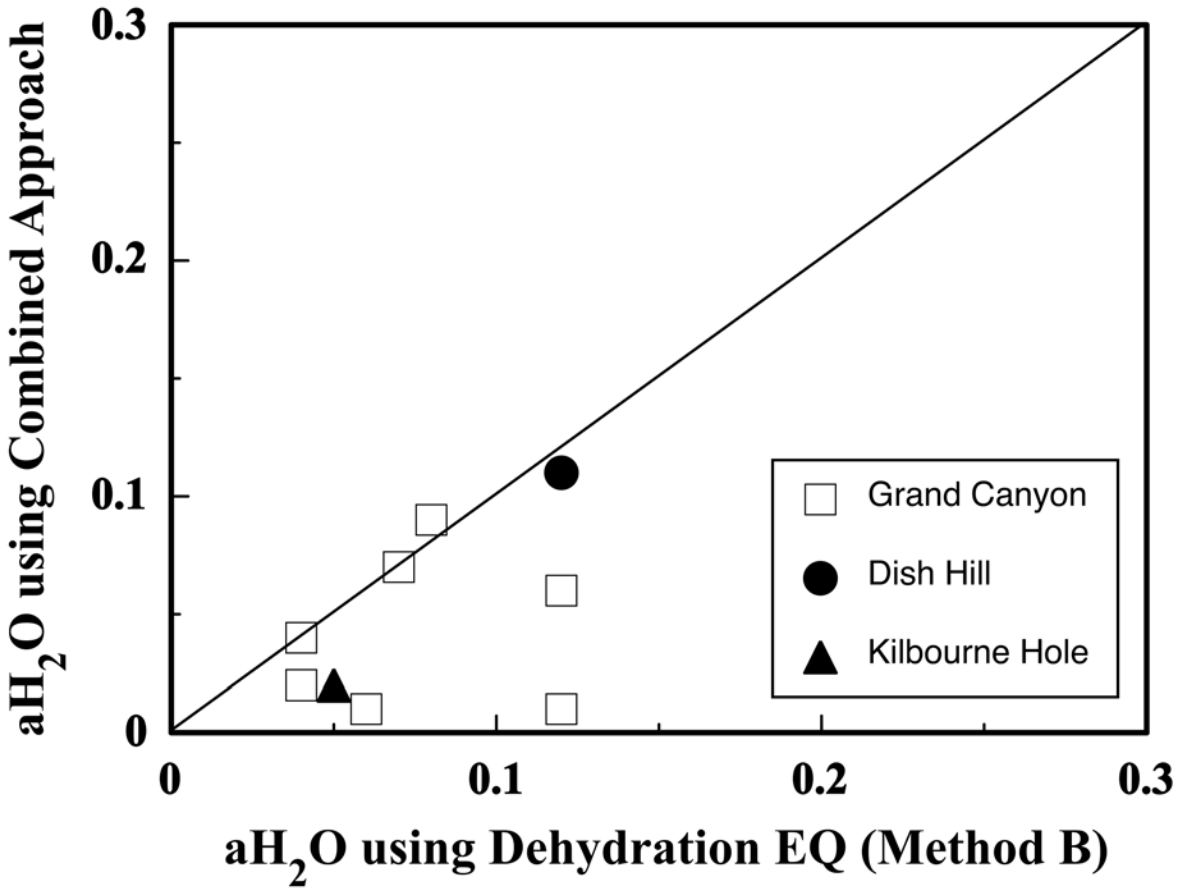

This is a preprint, the final version is subject to change, of the American Mineralogist (MSA)
Cite as Authors (Year) Title. American Mineralogist, in press.
DOI: https://doi.org/10.2138/am-2019-6602

Figure 7

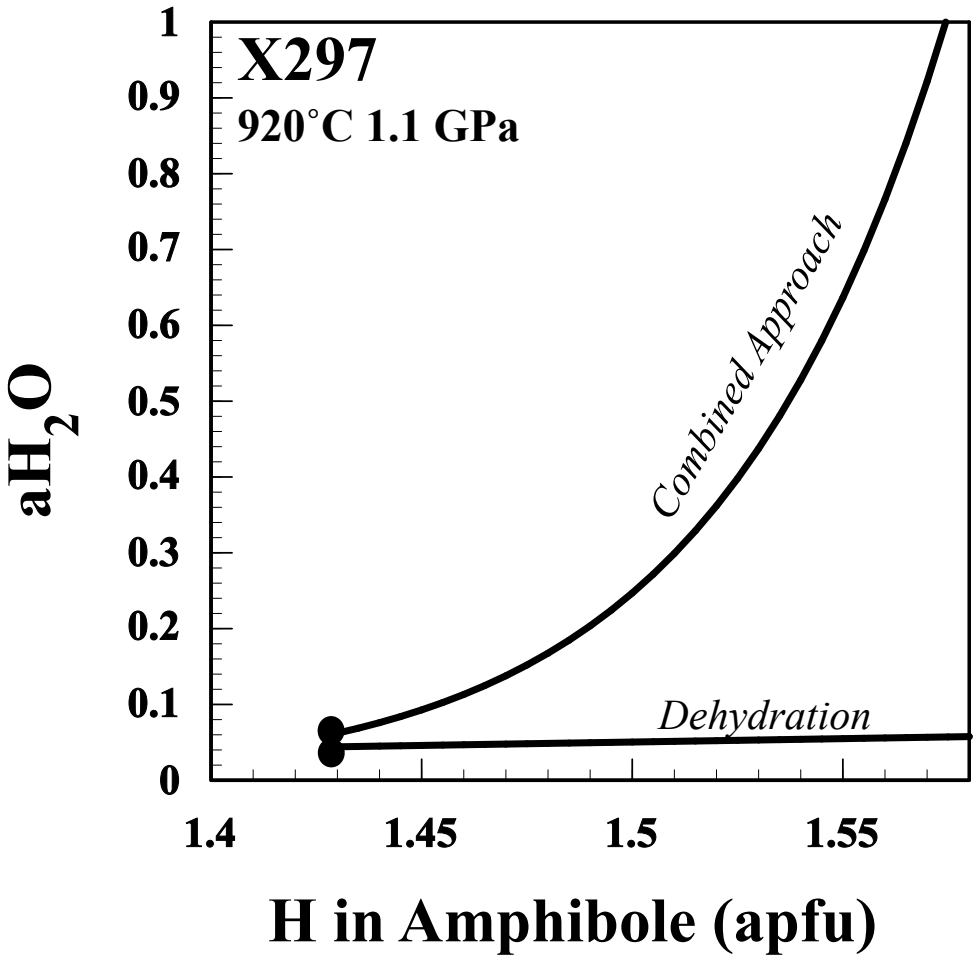

This is a preprint, the final version is subject to change, of the American Mineralogist (MSA)
Cite as Authors (Year) Title. American Mineralogist, in press.
DOI: https://doi.org/10.2138/am-2019-6602

Figure 8